Mechanics and control of the cytoskeleton in *Amoeba proteus*

Micah Dembo
Theoretical Biology and Biophysics, Theoretical Division, Los Alamos National Laboratory, Los Alamos, New Mexico 87545

ABSTRACT Many models of the cytoskeletal motility of *Amoeba proteus* can be formulated in terms of the theory of reactive interpenetrating flow (Dembo and Harlow, 1986). We have devised numerical methodology for testing such models against the phenomenon of steady axisymmetric fountain flow. The simplest workable scheme revealed by such tests (the minimal model) is the main preoccupation of this study. All parameters of the minimal model are determined from available data. Using these parameters the model quantitatively accounts for the self assembly of the cytoskeleton of *A. proteus*: for the formation and detailed morphology of the endoplasmic channel, the ectoplasmic tube, the uropod, the plasma gel sheet, and the hyaline cap. The model accounts for the kinematics of the cytoskeleton: the detailed velocity field of the forward flow of the endoplasm, the contraction of the ectoplasmic tube, and the inversion of the flow in the fountain zone. The model also gives a satisfactory account of measurements of pressure gradients, measurements of heat dissipation, and measurements of the output of useful work by amoeba. Finally, the model suggests a very promising (but still hypothetical) continuum formulation of the free boundary problem of amoeboid motion. By balancing normal forces on the plasma membrane as closely as possible, the minimal model is able to predict the turgor pressure and surface tension of *A. proteus*.

Several dynamical factors are crucial to the success of the minimal model and are likely to be general features of cytoskeletal mechanics and control in amoeboid cells. These are: a constitutive law for the viscosity of the contractile network that includes an automatic process of gelation as the network density gets large; a very vigorous cycle of network polymerization and depolymerization (in the case of *A. proteus*, the time constant for this reaction is ≈ 12 s); control of network contractility by a diffusible factor (probably calcium ion); and control of the adhesive interaction between the cytoskeleton and the inner surface of the plasma membrane.

INTRODUCTION

Debate about the mechanism of amoeboid motions has gone on since the last century (DeBruyn, 1947), but as yet the dynamical laws that govern these phenomena are largely unknown. Much of the problem has been that realistic mechanical theories, even of simple cases of amoeboid motion, are so complex as to defy conventional mathematical analysis. The recent advent of supercomputers and the associated technology to numerically solve complex models promises to fundamentally change this situation. In the present paper we draw up the heavy artillery of computational methodology and lay siege to a simple but extensively studied aspect of amoeboid motion: this is the fountain flow of the cytoplasm of the giant amoebae (mainly *Amoeba proteus* but also *Amoeba dubia* and *Chaos carolinensis*).

The ideal realization of the fountain flow is most closely approached in specimens of *A. proteus* that are of the monopodial[1] morphology under conditions when the specimen is on a nonadhesive substrate or when the specimen is attached to the substrate only by its tail (Mast, 1926; Allen, 1961*a* and *b*; Grebecki, 1984). These arrangements ensure that the organism is unable to exchange momentum with its surroundings. As a result, the external geometry and the internal flow of the cytoplasm of the specimen are almost axisymmetric and remain steady for long periods. The stable external geometry establishes an intrinsic or "physiological" frame of reference with respect to which measurements of position and motion in the interior of the amoeba can be made. Such a frame of reference allows quantitative comparisons between one specimen and the next and thereby leads to a statistically valid notion of what is typical or average. Equally important, if observations are to be subjected to theoretical interpretation, is the fact that an axisymmetric geometry allows one to avoid full three-dimensional computations. Furthermore, a fixed geometry allows one to avoid the full free boundary problem and to obtain simultaneously the advantage of very efficient and accurate numerical algorithms.

[1]Grebecki and Grebecka (1978) have critized use of the term "monopodial" and have proposed use of the term "orthotactic" as an alternative. This suggestion has considerable merit, but for the present discussion I will continue with the older convention.

0006-3495/89/06/1053/28 $2.00

MICROANATOMY OF MONOPODIAL *A. PROTEUS*

The kinematic features of the fountain flow as well as the important anatomical concepts of the endoplasmic channel, the ectoplasmic tube, the plasma gel sheet, the hyaline cap, and the uropod, are well known (Mast, 1926; Allen, 1961*a* and *b*; Allen, 1973; Grebecki, 1982). Nevertheless, for our purposes it have been necessary to supplement these accounts by a quantitative statistical analysis.

Fig. 1 *a* shows an accurate diagram of the "ideal" or average monopodial specimen of *A. proteus* in medial section. This figure was constructed by us based on raw data kindly supplied by Dr. A. Grebecki of the M. Nencki Institute in Warsaw. These data consist of micrographs of 25 specimens of *A. proteus* selected at random from cultures maintained in his laboratory. All micrographs had scale of 1 cm = 40 μm, 13 specimens were photographed in dark field and the rest in bright field, and various exposure times between 1 and 4 s were used. All specimens were suspended on nonadhesive substrata and underwent active fountain flow (see Grebecki, 1984, for details of methodology). Specimens that displayed signifi-

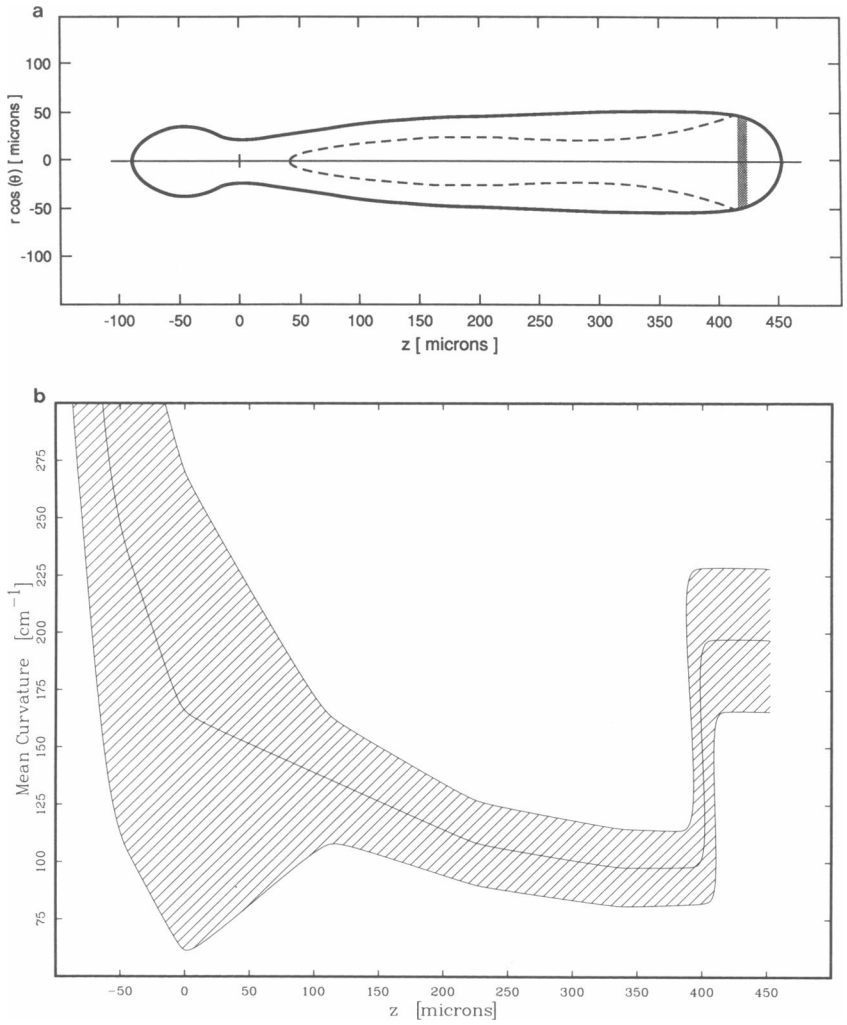

FIGURE 1 (*a*) Anatomy of monopodial *A. proteus*. The features of a composite or average specimen of monopodial *A. proteus* are represented in medial cross-section. Data consisting of 25 micrographs of actively streaming organisms on nonadhesive substrata were kindly supplied by A. Grebecki of the M. Nencki Institute in Warsaw. Radial symmetry about the z-axis is assumed and the orientation of the z-axis is such that z increases from posterior to anterior. (*Dashed line*) Boundary between endoplasm and ectoplasm; (*stipples*) plasma gel sheet. The hyaline cap corresponds to the region anterior of the plasma gel sheet. The region $z < 0$ is called the uropod and the thin segment encompassing the saddle-point near $z = 0$ is called the caudal cervix. (*b*) Mean curvature of external surface of *A. proteus*. $\bar{C}$ is given as a function of z. (*Solid line*) Average of all 25 specimens in Grebecki's sample. The shaded area corresponds to ± 1 SD. Expected value of the mean curvature at the posterior extremity (which lies off the scale) is equal to 866 cm^{-1}; the standard deviation at this point is $\pm 53\%$ of mean.

cant curvature of the midline (i.e., comma-shaped specimens) were not considered in the sample, nor were specimens that lacked visible frontal cap or that displayed small secondary pseudopodia or blebs. As a check on the validity of the sampling technique used to generate Fig. 1 *a*, we compared the results with a sample of 11 micrographs of monopodial *A. proteus* that have been published in various journals over the past 20 years. The external dimensions of the average organism in the latter sample were enlarged by a scale factor of 22%. If we adjusted for this scale factor, we could find no other significant differences between the two sample populations.

Some average measurements of *A. proteus* and the associated standard deviations follow. Distances are all given in microns and volumes in cubic microns. Standard deviations are expressed as plus or minus percentage of mean value. In all cases, the standard error of the mean is one fifth of the standard deviation (i.e., n = 25).

Axial distances:

Caudal cervix to anterior extremity (i.e., the length of the anterior body segment): 452.8 ± 13%
Caudal cervix to posterior extremity: 90.1 ± 40%
Caudal cervix to start of the endoplasmic channel: 41.1 ± 78%
Plasma gel sheet to anterior extremity: 30.0 ± 23%

Outer diameters:

At the midpoint of the uropod: 69.4 ± 32%
At the caudal cervix: 41.6 ± 26%
At one quarter of the anterior body: 78.8 ± 15%
At one half of the anterior body: 94.4 ± 10%
At three quarters of the anterior body: 104.9 ± 12%
At the plasma gel sheet: 91.4 ± 8%

Channel diameters:

At one quarter of the anterior body: 37.7 ± 30%
At one half of the anterior body: 45.6 ± 18%
At three quarters of the anterior body: 51.2 ± 17%

Volumes:

Of total interior: $3.03 \times 10^6 \pm 25\%$
Of ectoplasm: $1.80 \times 10^6 \pm 28\%$.

In subsequent developments (cf. section on boundary stresses) we will have reason to consider the analogy between the shape of a monopodial *A. proteus* and the shapes encountered in classical free boundary problems, such as the hanging drop problem or the meniscus problem. In other words, we will entertain the notion that the shape shown in Fig. 1 *a* is not an accident but is dictated by the requirement of balance between normal stress and surface stress. In the discussion of these free boundary problems, a geometric property of smooth surfaces called the mean curvature plays a central role. For the surface of an axisymmetric object such as the monopodial *A. proteus*, the mean curvature of a point is very easy to calculate according to the formula

$$\bar{C} = 0.5[(1./R_{mer}) + (1./R_{lat})], \quad (1)$$

where R_{mer} and R_{lat} are the radii of curvature along the meridionol and latitudinal geodesics, respectively. We adopt the convention that radii of curvature are taken to be positive if the center of curvature lies toward the inside of the cell. For a closed axisymmetric surface this means that R_{lat} is always positive because the center of curvature must lie on the axis; R_{mer} can be either positive or negative. For the case at hand (see Fig. 1 *a*), it is clear that R_{mer} is usually positive except near the caudal cervix. It is well to realize that the particular choice of meridional and latitudinal geodesics in Eq. 1 is a convenience for purposes of calculation and has nothing to do with the basic meaning of $\bar{C}$. This follows from a well-known result of Gauss to the effect that the mean curvature of any orthogonal pair of geodesics passing through a point on a smooth surface is the same.

Fig. 1 *b* shows the results of direct experimental determination of the expected value and standard deviation of $\bar{C}$. The figure was compiled by some further statistical massage of our measurements of Grebecki's photographs. To plot the results versus the "physiological" z-coordinate of the "average" specimen, we rescaled distance measurements on individual specimens before computing curvatures. For this purpose the mean distance from caudal cervix to anterior extremity of 453 μm was adopted as standard. The interpolation procedures used in numerically computing curvatures are essentially trivial and do not represent a significant source of statistical uncertainty or bias. The central curve in Fig. 1 *b* shows the average of the 25 independent measurements, and the shaded area corresponds to plus and minus one standard deviation. The coordinate system adopted to represent the results is the same as that of Fig. 1 *a* (i.e., origin of z-axis is at the caudal cervix).

One notices that $\bar{C}$ is very large and highly variable at the posterior. Both $\bar{C}$ and the variability of $\bar{C}$ drop sharply until the caudal cervix. $\bar{C}$ continues to decline gradually over the main anterior cylinder of the amoeba until a point ~50 μm posterior of the anterior tip. At this point $\bar{C}$ suddenly jumps by a factor of 2 and is thereafter constant until the anterior extremity. The abrupt jump in $\bar{C}$ corresponds to the point where the nearly perfect hemispherical cap at the anterior (see Fig. 1 *a*) is joined to the somewhat cylindrical domain of the central body.

GENERAL THEORY

Conservation laws

To our knowledge, the presence of intermediate filaments and/or microtubules in the cytoplasm of *A. proteus* or other giant amoebae has never been reported. Thus for the present analysis we shall be concerned with the dynamics of only two material phases: the filamentous network of actin, myosin, and various actin-binding proteins (Pollard and Ito, 1970; Pollard and Korn, 1971); and a second phase consisting of the aqueous solution that fills the rest of the available volume. A practical language for analyzing the mechanics of this situation is provided by the theory of interpenetrating reactive flow (Dembo et al., 1984; Dembo and Harlow, 1986). To apply this theory, let x_j be Cartesian coordinates and let f and $V_j^{(n)}$ be the volume fraction and velocity components of the network phase. Also, denote the velocity and pressure of the solution phase by $V_j^{(s)}$ and p, respectively, and the (Cartesian) rate of strain tensors for the network and solution phases by

$$E_{ij}^{(n)} \equiv \partial_{x_i} V_j^{(n)} + \partial_{x_j} V_i^{(n)} \tag{2a}$$

and

$$E_{ij}^{(s)} \equiv \partial_{x_i} V_j^{(s)} + \partial_{x_j} V_i^{(s)}, \tag{2b}$$

respectively.

In the case of fountain flow in *A. proteus*, it is known that both the Reynolds number of the motion and the volume fraction of the cytoskeleton are everywhere very much less than one (Allen and Roslansky, 1958, 1959). For simplicity, we will further restrict consideration to models in which the network phase behaves as an isotropic viscous or pseudoplastic fluid. With these simplifying assumptions we can proceed to write the equations for conservation of mass and momentum of the network and solution phases (Dembo and Harlow, 1986) in the form:

$$0 = \partial_{x_j} V_j^{(s)}, \tag{3a}$$

$$\partial_t f = -\partial_{x_j}[f V_j^{(n)}] + \mathscr{F}, \tag{3b}$$

$$0 = \partial_{x_j}[\mu_s E_{ij}^{(s)}] + f\mathscr{H}[V_i^{(n)} - V_i^{(s)} - \partial_{x_i} p, \tag{3c}$$

$$0 = \partial_{x_j}[f\mathscr{M} E_{ij}^{(n)}] + f\mathscr{H}[V_i^{(s)} - V_i^{(n)}] + \partial_{x_i}[f\mathscr{C}]. \tag{3d}$$

In many models of cell motion it is postulated that the local concentration of certain molecules or ions of low molecular weight strongly influence the fundamental chemical and rheological coefficients of the cytoskeleton. We will call small molecules that function in this way "cybernetic factors" because essentially their work is to encode spatial information for purposes of control. Calcium ion is the prime candidate for the role of cybernetic factors in *A. proteus*, but a role for other chemicals (e.g., ATP, H^+) has also been suggested (see review by Taylor and Condeelis, 1979). For models that include one or more cybernetic factors, Eq. 3, a–d, must be supplemented by additional equations to describe the diffusion, reaction, and convection of each such factor (see Appendix, Dembo and Harlow, 1986). If q and δ_q are respectively the concentration and diffusion constant of a cybernetic factor in the solution phase, then the relevant transport equation is

$$\partial_t q = -\partial_{x_j}[q V_j^{(s)}] + \partial_{x_j}[\delta_q \partial_{x_j} q] + \mathscr{S}. \tag{3e}$$

Although Eq. 3, a–e, embodies certain restrictive approximations, they are still extremely general. In particular, the five scalar coefficients ($\mathscr{F}$, $\mathscr{H}$, $\mathscr{M}$, $\mathscr{C}$, and $\mathscr{S}$) are completely unspecified. The manner of choosing the constitutive laws for these coefficients forms the main basis for distinction between different models of the cytoplasm and will be discussed subsequently.

Boundary conditions

Let Ω be an axisymmetric region chosen so as to approximate the experimentally determined geometry of the monopodial amoeba. The boundary of Ω can be divided into three segments: the anterior boundary (corresponding roughly to the segment of plasma membrane enclosing the hyaline cap), the posterior boundary (corresponding to the plasma membrane at the uroid), and the lateral boundary (corresponding to the rest). We denote these three segments by $\partial\Omega_a$, $\partial\Omega_p$, and $\partial\Omega_l$, respectively. In certain plausible models these three boundary surfaces have intrinsic differences due to variation of the material properties of the associated segments of cell membrane.

Let L_j and N_j be components of a unit tangent and outward-normal vector on one of the three boundary surfaces. The boundary in question is said to be "slip" with respect to tangential velocity components if

$$E_{ij}^{(s)} N_i L_j = E_{ij}^{(n)} N_i L_j = 0, \tag{4a}$$

and "no-slip" if

$$L_j V_j^{(s)} = L_j V_j^{(n)} = 0. \tag{4b}$$

The water permeability of the plasma membrane of fresh water amoebae is $\approx 2 \times 10^{-14}$ ml/dyn per s, and the osmotic concentration of the cytoplasm is the equivalent of ~94 mM of ideal nonelectrolyte (Lovtrup and Pigon, 1951). It can then be calculated that the passive flux of water into an amoeba maintained in Pringsheim medium is only a few percent of the cell volume per hour. Obviously, this amount must simultaneously be removed by the functioning of the contractile vacuole for the amoeba to maintain constant volume. In any event,

because the permeability and the water fluxes are quite negligible, we take

$$N_j V_j^{(s)} = 0 \tag{4c}$$

as the only possibility for the boundary condition on the normal component of the solution velocity. There are two important possibilities for the corresponding boundary condition on the network. A boundary segment is said to be "stick" with respect to the network velocity if

$$N_j V_j^{(n)} = 0 \tag{4d}$$

at all points. The boundary is said to be "no-stick" if

$$E_{ij}^{(n)} N_i N_j = -\mathcal{C}/\mathcal{M}, \tag{4e}$$

subject to the constraint $N_j V_j^{(n)} \leq 0$.

Finally we can restrict consideration to cases in which the boundary conditions for q on a boundary segment are either Neumann,

$$[qV_j^{(s)} - \delta_q \partial_{x_j} q] N_j = \text{const}, \tag{4f}$$

or Dirichlet,

$$q = \text{const}. \tag{4g}$$

In the case of the q boundary condition, both the type of boundary condition and the value of the associated constant are chosen independently on the anterior, posterior, and lateral surfaces of Ω.

Because we regard the boundaries of the amoeba as rigid and impenetrable to volume fluxes, the pressure field inside the amoeba is only determined up to an arbitrary additive constant (i.e., only gradients of pressure appear in the governing PDEs). As a matter of definition we take this additive constant such that the lowest value of the p at any point in Ω is equal to zero. Thus p, by definition, is a relative pressure. The absolute pressure is

$$p_{\text{abs}} = p + p_{\text{ext}} + p_0, \tag{5}$$

where p_{ext} is the pressure in the external medium and p_0 is the pressure jump between the point of minimum pressure inside the cell and the exterior. p_0 is a measurable quantity corresponding to what is usually called the "turgor" pressure. The turgor pressure is determined by many factors: the hydraulic conductivity of the plasma membrane, the osmolarity of the internal and external media, the activity of the contractile vacuole, etc. Nevertheless, based on certain considerations related to the balance of boundary stresses, we shall subsequently compute its value (cf. section on boundary stresses).

With one important exception the various boundary conditions that we have considered for the network and solution phases and for the cybernetic factor are familiar to anyone conversant with continuum mechanics. The exception is the so-called no-stick condition (Eq. 4e); it is crucial because it seems to be the main basis for the development of anterior/posterior polarity in monopodial *A. proteus* (cf. Discussion). The no-stick condition is unusual because of the associated constraint.

From a qualitative point of view, the dynamical description of the no-stick boundary is extremely simple. If network material close to the boundary moves toward the inside of the cell, then the boundary offers no resistance. If network material near the boundary attempts to move outward, the boundary presents an impenetrable obstacle and the constraint comes into play. In a biophysical context, this sort of behavior is precisely what one expects at a portion of the inner surface of the plasma membrane, which has few adhesive sites for anchorage of the cytoskeleton. If the quantitative formulation of the no-stick condition seems opaque, the derivation offered by Dembo and Harlow (1986) may be helpful.

NUMERICAL METHODS

After converting Eq. 3, a–d, to finite difference form, one obtains a large system of nonlinear algebraic equations for the discrete field variables. The overall computational procedure we employ for solving these equations is one of block relaxation (Young, 1971). The blocks we employ correspond to the "natural" partitioning of the algebraic equations and field variables: pressure and Eq. 3a, network density and Eq. 3b, solution velocity and Eq. 3c, network velocity and Eq. 3d, and concentration of cybernetic factor and Eq. 3e. Individual subroutines are used to adjust or improve the part of the overall solution corresponding to each block. In each of these subroutines the field variables other than the one under adjustment are viewed as fixed. The subroutines are repeatedly executed in a cyclical fashion until a convergence criterion is satisfied, but with a minimum of three cycles required on each time step. Convergence is accelerated and stability enhanced by use of underrelaxation. In the subsequent description of the individual subroutines, variables and spatial differences based on axisymmetric spherical coordinates are implied.

The time derivatives of the continuity equations for the network and cybernetic factor are differenced according to the Crank-Nicolson procedure: convective terms are differenced according to the upwind difference scheme with second order advection in the case of the network and with simple donor cell advection in the case of cybernetic factor. Diffusive terms in the transport equation of the cybernetic factor are differenced by application of the finite difference form of Ficks' law. The duration of the time step was adaptively adjusted during computations so as to satisfy the Courant condition by a constant factor.

Experience has shown that a major limitation of accuracy of the final results is the spatial resolution of rapid variations of the network density field. Accordingly, the grid spacing for the network density field is half that used for the other variables. This necessitates some interpolation to compute the components of the network velocity at the edges of the network density grid cells. The algebraic equations resulting from the discreteization of the continuity equations for network and cybernetic factor are very well conditioned, and simple Jacobi iteration was adequate for their solution.

The equations for force balance on the network and solution are discretized according to the nine-point finite difference scheme for staggered grid in spherical coordinates. This method is well known and was originally introduced in the "marker and cell" method (Harlow and Welch, 1965). The method was extended to low Reynolds number flows by Pracht (1971), who introduced the use of fully implicit (i.e., time-advanced) velocity components for discreteization of the viscosity terms. For the present case, care must be taken with the arrangement of grid cells so that no artificial sources or sinks for momentum occur at the axis of symmetry. It is also necessary to multiply the equations for the two components of momentum by scaling factors in such a way that the matrix resulting from the discreteization is symmetric, positive, definite, and well conditioned. Solution of the algebraic equations are then efficiently obtained by means of the preconditioned conjugate gradient method (Stoer, 1983).

A Poission equation for the pressure is obtained by taking the divergence of the momentum equation for the solution and applying the condition of incompressibility. This equation is then discretized according to the usual five-point finite difference scheme (Pracht, 1971) and the resulting algebraic system solved by the conjugate gradient method.

Boundary conditions are essentially trivial to apply except in the case of the no-stick conditon. This condition requires that one make laborious checks on the tendency of the network to move inward or outward at each point along the boundary. To determine this tendency one starts with the assumption that the tendency will be to move inward at all points and looks for violations of this assumption. If a violation is found, then one must apply the constraint that prevents outward flux at the boundary point in question; if a previous tendency to move outward ceases, then one must be prepared to remove the constraint. These checks and rechecks must be done during each cycle of the time step iteration until a consistent solution emerges.

The overall algorithm was checked for mass, momentum, and energy conservation, and for agreement with standard benchmark computations reported previously (Dembo et al., 1986). Cauchy convergence of computations subsequently discussed was indicated by the fact that changes in spatial or temporal resolution by a factor of two had no appreciable effect on the results. In the benchmark computation (cf. comparison with experiment) the basic grid for pressure, cybernetic factor, and velocity, including boundary cells, is 16 by 64.

MINIMAL MODEL

To convert the general theory we have presented into a specific model, we must provide constitutive relations for the scalar functions $\mathcal{J}$, $\mathcal{H}$, $\mathcal{M}$, $\mathcal{C}$, and $\mathcal{S}$. These functions describe the rate of network polymerization (or depolymerization), the specific hydraulic resistance of the network, the specific shear viscosity of the network, the specific contractile stress of the network, and the chemical production (or destruction) of q in the cytoplasm, respectively. We must also specify which of the many possible choices for boundary conditions are to be used on the anterior, posterior, and lateral surfaces of Ω. There are an infinite number of variations; of those we have tested, many are quite successful at accounting for the known properties of *A. proteus*, and many more are failures. To understand the essential elements that distinguish success from failure, let us consider the simplest satisfactory model that we have yet been able to devise (the minimal model). This model employs the following constitutive relations:

$$\mathcal{J} = [\rho_{ceq} - f]/\tau_n \tag{6a}$$

$$\mathcal{H} = \mu_s/\kappa \tag{6b}$$

$$\mathcal{M} = \mu_n \exp[(f/\rho_{gel})^2] \tag{6c}$$

$$\mathcal{C} = \psi[q - \xi] \tag{6d}$$

$$\mathcal{S} = -q/\tau_q. \tag{6e}$$

The constitutive law for $\mathcal{J}$ means that the chemical synthesis and breakdown of the network is governed by simple linear mass action. The constant parameters ρ_{ceq} and τ_n correspond to the volume fraction of network at chemical equilibrium and the relaxation time of the reaction, respectively. Implicit in this constitutive law for $\mathcal{J}$ is the notion that the monomeric or oligomeric precursors of the network are in constant supply and uniformly distributed and that the reaction is not controlled by cybernetic factor.

The constitutive law for $\mathcal{H}$ means that the hydraulic drag between the network and solution phases follows Darcy's law for flow through porous media (the constant κ is the permeability coefficient). A simple discussion of

hydraulic drag between aqueous fluids and filament networks is given by Happel and Brenner (1973). These authors show that κ is, in general, a measure of the cross-sectional area of the typical filament of the network and that κ is only very weakly dependent on network geometry and density.

The constitutive law for $\mathcal{M}$ is meant to empirically describe the effects for formation of cross-links between network filaments. If f is below ρ_{gel} (the "gel point"), then the specific viscosity is simply a constant. As f gets much larger than the gel point, however, the specific viscosity increases explosively. Thus, as used in the minimal model, the concept of gelation is rather limited and simply connotes a very large increase in the effective viscosity of the network (i.e., a thickening). Gelation does not imply that a true elastic contribution to the network stress suddenly comes into existence. Implicit in this usage is the idea that the cross-links that lead to gelation are noncovalent and easily broken. Furthermore, since the gel point is taken to be constant independent of position and time, it is implicitly assumed that the "activity" of the molecules responsible for cross-linking of filaments is controlled only by the network density itself and not by cybernetic factors. Finally, the processes of network cross-linking described by the constitutive law for $\mathcal{M}$ should not be confused with the processes of actual synthesis and breakdown on network embodied in $\mathcal{J}$.

The constitutive law for $\mathcal{C}$ embodies the assumption that the contractile tendency of the network filaments is a linear function of the concentration of cybernetic factor. The law is expressed in terms of a constant of proportionality, ψ, as well as a parameter, ξ (the contraction threshold). The latter gives the amount of cybernetic factor at which contraction exactly balances the osmotic expansion or swelling of the network. In the minimal model it is most convenient to express the concentration of cybernetic factor in nondimensional units. (Subsequently the maximum value of q in the interior of the amoeba is adopted as the natural unit of concentration.) As a result, ξ is also nondimensional; and the parameter ψ, which has units of dynes per centimeter squared, is called the characteristic contractile stress.

The final constitutive law used in the minimal model, that for $\mathcal{S}$, prescribes a simple linear decay of cybernetic factor due to sequestration or enzymatic degradation within the bulk of the cytoplasm. The parameter τ_q is the characteristic lifetime of the cybernetic factor. Because no interior sources of q are included in $\mathcal{S}$, use of this simple constitutive law implies that there must be a supply of q at the boundaries if one is to obtain nontrivial solutions.

For the region Ω the minimal model takes a right circular cylinder of length l_Ω and ratius r_Ω. For future reference, the origin of cyclindrical coordinates (r, θ, z) is taken at the center of the posterior surface; the anterior surface coincides with the plane $z = l_\Omega$. This should not be confused with the coordinate system used for Fig. 1, *a* and *b*, wherein the origin was taken at the caudal cervix.

The tangential and normal boundary conditions for the velocity fields in the minimal model are slip/no-stick on the anterior surface, and slip/stick on both the lateral surface and the posterior surface. The q-boundary conditions of the minimal model are Dirichlet (Eq. 4g) with constant equal to one on all three boundary surfaces. This choice of the constant involves no real loss of generality because the boundary value would in any case be used as the natural scale for nondimensionalization of q.

If one includes the length and radius of Ω, there are 12 parameters in the full dimensional form of the minimal model. These parameters, together with our best estimate of their values in a typical amoeba, are listed in Table 1.

Three of the parameters in Table 1 have been either directly measured or can be determined with sufficient accuracy from measured quantities on the basis of theoretical arguments that are model independent. l_Ω and r_Ω are average quantities obtained from direct measurements and rounded off for simplicity (see Fig. 1 *a*). The diffusion coefficients of three extrinsic probes, ribonuclease A, ovalbumin, and bovine serum albumin, have been measured in aqueous solution and in the cytoplasm of *A. proteus* using the FRAP technique (Wang et al., 1982). Because the diffusion coefficient is inversely proportional to viscosity, these measurements yield the indicated value of μ_s.

Three more parameters of Table 1 are determined if we adopt the view that the cybernetic factor is one and the same as calcium ion. The value of δ_q is computed from the

TABLE 1 Parameters of the minimal model

Parameter	Symbol	Value	cgs units
Length of Ω	l_Ω	5.0×10^{-2}	cm
Radius of Ω	r_Ω	5.0×10^{-3}	cm
Solution viscosity	μ_s	3.0×10^{-2}	poise
Volume fraction of network at chemical equilibrium	ρ_{ceq}	7.2×10^{-3}	—
Characteristic lifetime of network elements	τ_n	1.2×10^{1}	s
Viscosity of network (at $f = 0$)	μ_n	1.2×10^{3}	poise
Volume fraction of network at gel point	ρ_{gel}	5.4×10^{-3}	—
Characteristic contractile stress of network	ψ	1.8×10^{4}	dyn/cm^2
Network permeability	κ	2.5×10^{-11}	cm^2
Diffusion constant of cybernetic factor	δ_q	3.7×10^{-6}	cm^2/s
Characteristic lifetime of cybernetic factor	τ_q	8.4×10^{-1}	s
Contraction threshold	ξ	1.4×10^{-1}	—

measured diffusion coefficient of calcium chloride in water by applying the correction for solvent viscosity. The value of the nondimensional contraction threshold, ξ, is taken equal to the ratio between the calcium concentration in "relaxation solution" and the calcium concentration in "flair solution" (Taylor et al., 1973). This estimate is based on in vitro studies of isolated cytoplasm. However, the result is supported by direct measurements of intercellular calcium (Taylor et al., 1980*a*). The value of τ_q is determined with sufficient accuracy from stability constraints (cf. next section).

The pieces of data used to fix the remaining six parameters of the minimal model are as follows: (*a*) stability and existence of the plasma gel sheet; (*b*) the diameter of the endoplasmic channel at the midpoint; (*c*) the contraction rate of the ectoplasm at the midpoint; (*d*) the difference in volume fraction of network in ectoplasm versus endoplasm as determined by measurements of refractive index; (*e*) the viscosity of the endoplasm as measured by the magnetic particle technique; and (*f*) the percentage of the volume of the amoeba that is ectoplasm. These data are discussed in more detail in the subsequent section. For the present, therefore, we shall simply assert that if one believes the minimal model and if one believes the existing information concerning the properties of fountain streaming in *A. proteus,* then one is forced to accept the numbers given in Table 1, modulo the usual biological variability of 10–50%.

COMPARISON WITH EXPERIMENT

Morphology

We now consider the numerical solution of the minimal model for the case of the parameter values shown in Table 1. A low-resolution overview of this computation at a fixed instant of time is given in Fig. 2. More detailed plots of special aspects of the computation are given in subsequent figures as needed.

The solution shown in Fig. 2 is a completely stable steady state established within $\approx$1 min starting from initial conditions in which the distribution of q and f are completely uniform in Ω. This means that the indicated solution of the minimal model has the property of "self assembly." The existence of such highly stable solutions is a necessary aspect of satisfactory models.

From the contour plot of f in Fig. 2, one can verify that the gross morphological features of the distribution of the cytoskeleton in monopodial *A. proteus* are reproduced by the minimal model in a quantitative fashion (simply compare Figs. 1 *a* and 2). At the anterior extremity there is a region of very low network density (the hyaline cap). Posterior of this lies a thin ridge of relatively high network density completely spanning the cross-section of the amoeba from axis to lateral boundary (the plasma gel sheet). Along the midsection of the amoeba, underlying the lateral boundary, there is a thick region of high network density (the ectoplasmic tube). The tube contains a cyclindrical domain of low network density (the endoplasmic channel). At its anterior extremity the endoplasmic channel gradually widens and the walls of the ectoplasmic tube correspondingly narrow. At its posterior extremity, the endoplasmic channel collects from an irregular region consisting of interwoven subareas of high and low network density.

The expected value of the percent ectoplasm in Grebeckis' sample (see Fig. 1 *a*) is 59.4 $\pm$ 3. The parameters of Table 1 have been chosen so as to insure that the percent of ectoplasm in Fig. 2 is within the experimental error.

The most delicate and controversial cytoskeletal structure in *A. proteus* is undoubtedly the plasma gel sheet; this is also the most difficult structure to explain theoretically. When Mast (1926) originally described the plasma gel sheet, he was careful to point out that its existence was simply inferred from the behavior of cytoplasmic granules; it was not actually visualized. Furthermore, in the past Allen has disputed the existence of the plasma gel sheet as a real anatomical object. Even among those who agree that it exists, there have been disputes as to the composition of the plasma gel sheet. In particular, there have been claims that in some specimens of *A. proteus* the frontal caps are simply large vacuoles and that the plasma gel sheet is thus actually a lipid membrane (see Grebecki and Grebecka, 1978).

In our view, the definitive proof of the existence of the plasma gel sheet and of its cytoskeletal composition was only obtained recently by visualization of the distribution of fluorescently labeled actin in living amoebae (Taylor et al., 1980*b*). The claims of frontal vacuoles in a small percentage of specimens cannot be disproved but have yet to be definitively verified.

In Fig. 2 the position of the plasma gel sheet is revealed by a thin contour of network density joining the axis with the anterior end of the ectoplasmic tube. The amplitude of the peak in network density at the center of the plasma gel sheet is about three times greater than the network density in the endoplasm, but even so the jump in density is probably an understatement of the true situation. This is because the thickness of the plasma gel sheet is comparable with the spacing of grid points, and there is thus some unavoidable numerical smoothing of this portioin of the solution. The distance between the center of the plasma gel sheet and the anterior extremity is seen to be $\approx 3.5 \times 10^{-3}$ cm. This number is within one standard deviation of the measured average for monotactic *A. proteus* in Grebecki's sample (see Fig. 1 *a*). In the minimal model, the plasma gel sheet occurs because of a

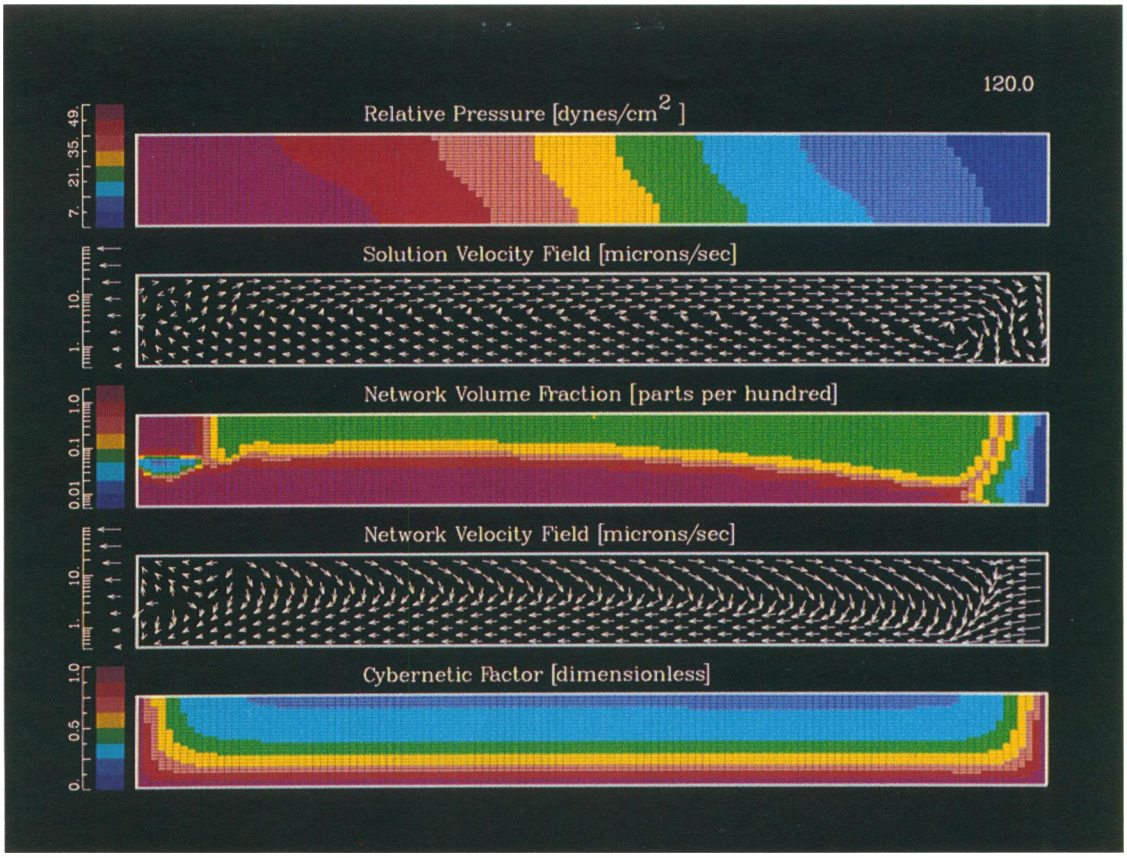

FIGURE 2 Steady fountain streaming according to the minimal model. False color contour maps are used to represent the scalar fields q, f, and p. The size of the rectangular pixels that compose the contour maps correspond to the numerical grid used in the computation; no interpolation or smoothing has been attempted. Vector maps are used to show $V_j^{(n)}$ and $V_j^{(s)}$ at locations spaced with a checkerboard pattern throughout the computational field. Each map represents only the lower half of a medial section through the cylindrical domain Ω (500 μm long and 50 μm in radius). The posterior extremity lies to the left and the anterior to the right. Scales that allow quantitative interpretation of the various maps appear immediately to the left; these are self-explanatory. A label designating each map and giving the units of the associated scale is written above the z-axis. As always, radial symmetry about the z-axis is assumed. The indicated solution of the minimal model is a completely stable steady state that is generated in $\approx$1 min starting from uniform starting distributions of both network and cybernetic factor. Parameters used in the computation are given in Table 1.

balance between hydraulic drag forces exerted on the network by the flow of the solution phase and contractile and viscous stresses of the network itself. The hydraulic forces try to push the network toward the anterior while the contractile and viscous stresses pull the network away from the anterior because of the boundary condition. If one or the other of these factors is too strong, then the plasma gel sheet will not occur or will occur in the wrong location. The existence and location of the plasma gel sheet is thus very useful to fix the parameters in Table 1.

Fig. 3 shows the predictions of the minimal model concerning the variation of network volume fraction with radius at anterior, posterior, and middle cross sections. Note the very sharp gradients separating endoplasm and ectoplasm. By measuring differences in refractive index, Allen et al. (1962) were able to estimate the ectoplasm-endoplasm difference in network volume fraction near the midpoint of a typical amoeba. The value found was $\approx$0.011; the parameters of Table 1 are determined so that the computed difference agrees exactly with this number.

Yagi (1961) has reported measurements of the ratio between endoplasm and ectoplasm at the midpoint of monotactic *A. proteus* (i.e., at a cross-section halfway between the anterior and the caudal cervix). The results can be expressed as a ratio between the radius of the endoplasmic channel and total radius of the organism. The expected value of the radius ratio in Yagi's study was 0.57 (SD $\pm$ 0.06, n = 14). This agrees well with the data of Mast and Prosser (1932) and Grebecki (Fig. 1 *a*). The parameters in Table 1 are chosen so that the computed value of the midpoint radius ratio is within the experimental error (see Fig. 3).

If the ectoplasm of the amoeba is contracting as

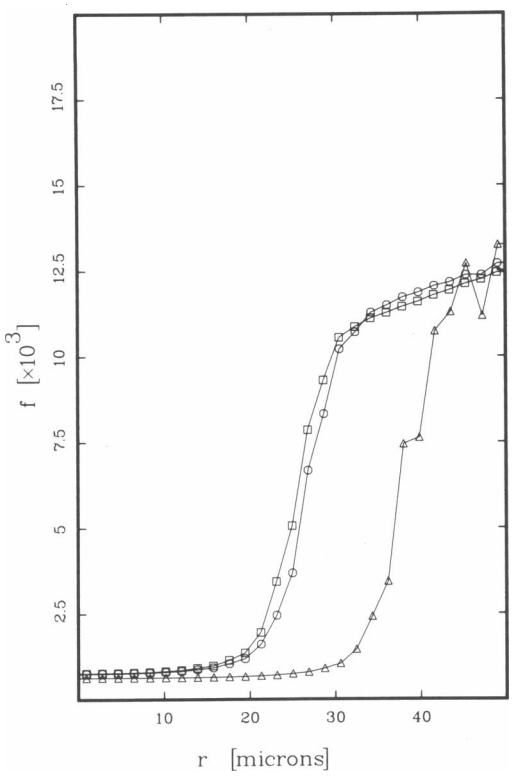

FIGURE 3 f versus r at three values of z. Shown are the predictions of the minimal model for the network volume fraction as a function of r for three different cross-sections: z = 100 μm (*squares*), z = 250 μm (*circles*), and z = 400 μm (*triangles*). Note the sharp gradients of network density separating regions of endoplasm and ectoplasm. As observed experimentally, the width of the endoplasmic channel is approximately half the total diameter at the midpoint of the amoeba. There are considerable differences in the proportions of endoplasm and ectoplasm at different values of z, but the average composition of the ectoplasmic and endoplasmic regions remains fairly constant. As reported by Allen et al. (1962), the ectoplasm-endoplasm difference in network volume fraction is ~0.011.

predicted by Mast (1926), then, assuming constant mass, one would expect the volume fraction of network in the ectoplasm at the posterior to be considerably larger than at the anterior. To test this notion, Allen and Francis (1965) made measurements of the refractive index of only the ectoplasmic portions of the cytoplasm. Although measurements were made in a large sample, they could detect no significant anterior-posterior differences in ectoplasmic composition. From Fig. 3 it can be seen that at any cross-section the cytoplasm can be divided roughly into zones of endoplasm and ectoplasm. The proportions of endoplasm and ectoplasm vary in different cross-sections, but the volume fraction of network in the ectoplasmic zone and the volume fraction in the endoplasmic zone remain fairly constant. This shows that the minimal model is consistent with the measurements of Allen and Francis.

It is worth mentioning that the constancy of the ectoplasmic density has recently been redemonstrated by some very beautiful images obtained with the holographic microscope (Opas, 1980). This study also failed to detect any significant differences in composition of the axial endoplasm from one end of the channel to the other.

Allen and Roslanski (1958) have reported measurements of the average refractive index of the combined endoplasm and ectoplasm at different positions from posterior to anterior. These measurements are indicative of the anterior-posterior changes in the ratio of endoplasm to ectoplasm predicted by the minimal model. For an average individual in the population studied by Allen and Roslansky, the anterior-posterior difference in average refractive index corresponded to a change of -0.0056 (SD $\pm$ 0.0030; n = 15) in the volume fraction of protein (note the negative sign). The root-mean-squared variation in volume fraction of protein between the anterior, posterior, and midpoint cross-sections was 0.0029 (SD $\pm$ 0.0017; n = 12). The corresponding theoretical predictions, based on the three sections indicated in Fig. 3, are -0.0033 and 0.0015, respectively.

Kinematics

Most of what is known of the kinematics of the fountain flow comes from the observation of cytoplasmic granules of $\leq$ 1 μm diameter. In the subsequent discussion we will assume, as a rule of thumb, that because network is present in small amounts, cytoplasmic granules track mainly the solution velocity field with only a small component proportional to the network velocity. The trajectories of the cytoplasmic granules of *A. proteus* are also undoubtedly influenced to some unknown degree by steric interactions that tend to exclude them from regions of high network density (Mast, 1926; Luby-Phelps and Taylor, 1988). Regardless of the detailed dynamical rules for tracer particles, it can be verified from the vector plots of the network and solution velocity fields in Fig. 2 that the minimal model successfully explains the main kinematic features of fountain streaming: the forward flow of the endoplasm and the backward flow of the ectoplasm. We now consider such matters in more detail.

In the frontal-contraction model of the fountain flow (Allen, 1961*a*), the forward flow of solution phase material in the endoplasm is driven by the contraction of network filaments aligned parallel to the axis. As a result, this model predicts a forward flow of both the solution and the network phases near the center of the endoplasm. In additon, the frontal contraction model predicts that the forward flow of the network should be faster than the flow of the solution phase (Odell, 1977). Fig. 4 *a* shows the corresponding predictions of the minimal model. The minimal model concurs in predicting a forward motion of

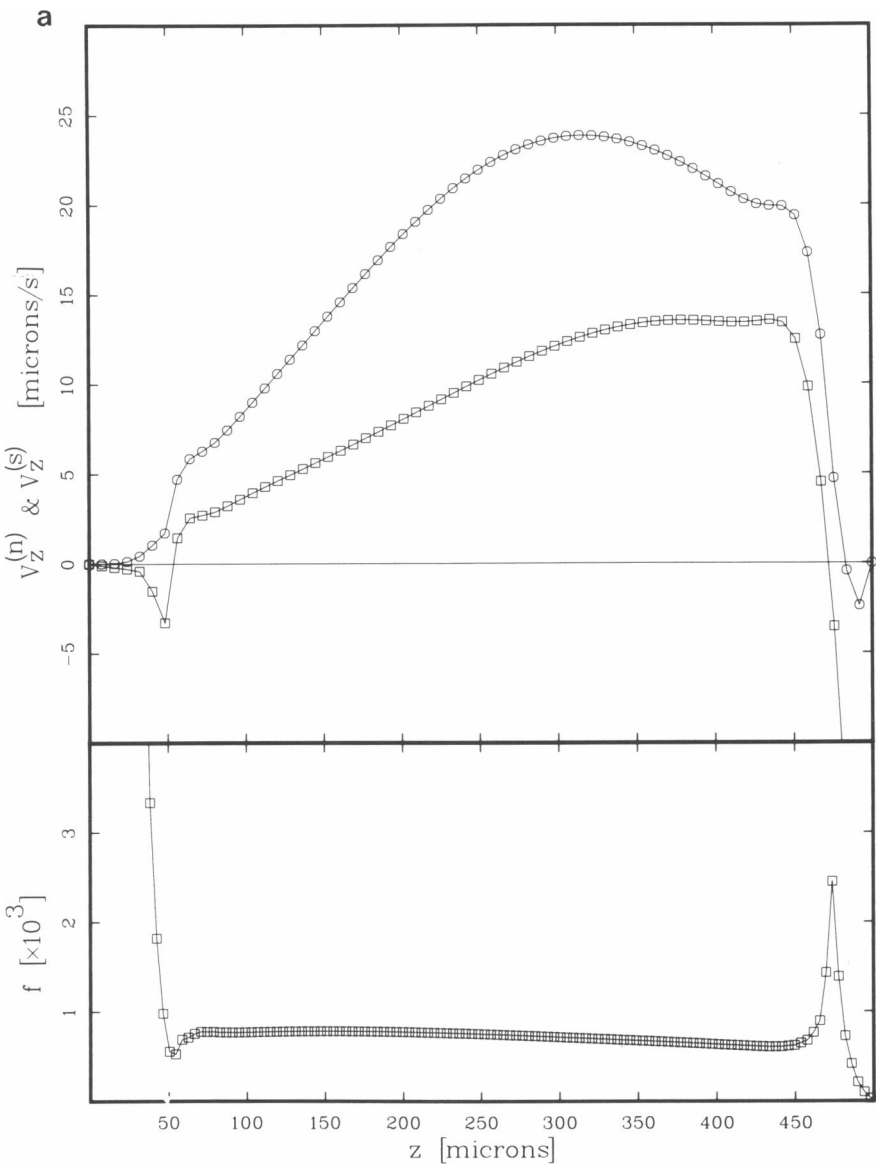

FIGURE 4 (*a*) $V_z^{(n)}$ and $V_z^{(s)}$ versus z at $r = 0$ μm. Predictions of the minimal model for network velocity (*squares*) and solution velocity (*circles*) at the axis are shown as a function of z. For purposes of orientation with respect to cytoskeletal structures, a graph of the network volume fraction at the axis is shown beneath the main graph. Both solution and network velocities are positive in the endoplasmic channel but drop to zero near the plasma gel sheet and become negative inside the hyaline cap. The reversal of solution velocity is due to the vortex inside the hyaline cap (see Fig. 2) and is a part of the explanation of the complex trajectories of tracer particles in the fountain zone (see text). From the graph of network volume fraction it is seen that the minimal model predicts the occurrence of a small region of extremely high network density (i.e., ectoplasm) at the posterior. The start of the endoplasmic channel is heralded by a drop in the network volume fraction to a value of $\approx 7 \times 10^{-4}$. There is then a further gradual decline in network density along the length of the channel with a relative minimum occurring near the center of the fountain zone. After this there is a sharp peak in network density corresponding to the plasma gel sheet. The network volume fraction then declines sharply and approaches very close to zero inside the hyaline cap. (*b*) $V_z^{(n)}$ and $V_z^{(s)}$ versus z at $r = 50$ μm. Network velocity (*squares*) and solution velocity (*circles*) at the lateral boundary are shown as a function of z. To provide orientation with respect to the cytoskeletal distribution, the network volume fraction at the lateral boundary is plotted beneath the main graph. Within the ectoplasmic tube there is a linear variation of network velocity with position; this implies a constant rate of network contraction (Grebecki's rule). The network and solution velocities in the ectoplasm are almost identical. The minimal model predicts a constant level of network density at the posterior and within the ectoplasmic tube. Near the anterior there is a sharp drop in network density corresponding to opening of the ectoplasmic tube and the start of the hyaline cap.

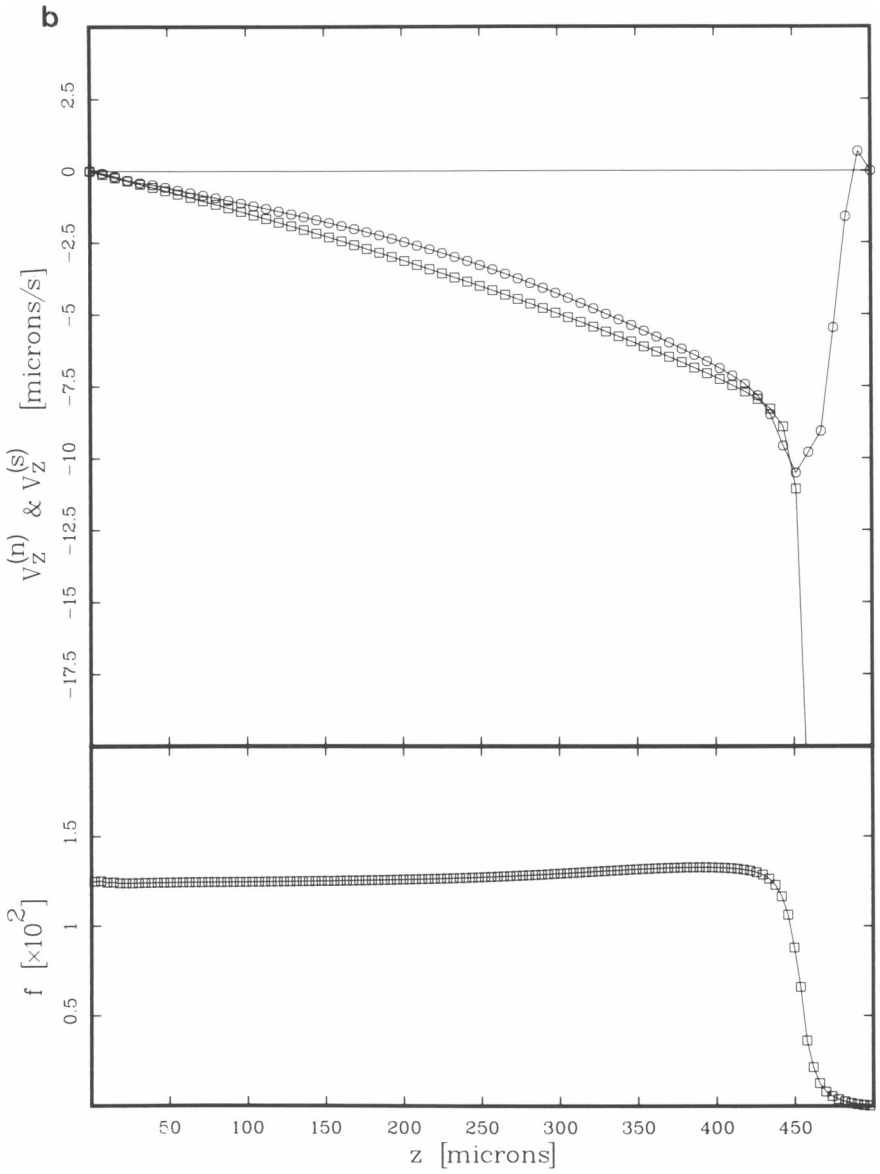

FIGURE 4 Continued

both solution and network in the endoplasm but makes exactly the opposite prediction concerning the relative velocities of endoplasm and ectoplasm. In other words, Fig. 4 *a* indicates that there are filaments in the endoplasm and that they flow toward the anterior, but the forward flow of the network is being driven by the motion of the solution phase and not vice versa. The actual motive force driving the endoplasmic flow in the minimal model is the pressure gradient produced largely by contraction of the ectoplasmic tube. In this very important respect the minimal model is in agreement with the model of Mast (1926). The latter is usually called the tail-contraction or the ectoplasm-contraction model.

The most complex details of the fountain flow occur in the region just posterior of the hyaline cap (this has been called the "fountain zone" [Allen, 1961 *a* and *b*]). As the granular endoplasm approaches the plasma gel sheet, particles in the central stream decrease their forward motion and accelerate laterally. They are thus ultimately deposited at the anterior end of the ectoplasmic tube. With some important exceptions (see below) they do not pass more than a few microns beyond the plasma gel sheet.

It was Mast's opinion that particles were prevented from entering the hyaline cap simply because the plasma gel sheet presented a static filtration barrier. This is

certainly a possible mechanism, but according to the minimal model one can also explain the trajectories of particles in the fountain zone by a completely separate (and complementary) mechanism. It can be seen from Fig. 2 that there is a vortex of solution flow inside the hyaline cap with rotation counter to that of the fountain flow itself. This is why the z-component of solution goes to zero a few microns anterior of the plasma gel sheet and actually becomes negative inside the hyaline cap itself (see Fig. 4 *a*). The counter vortex has the effect of bending the stream lines near the axis so that even if the plasma gel sheet were completely transparent to particles, the flow simply cannot carry particles into the hyaline cap.

In its simplest form the fountain flow is steady and continuous, but in some specimens cyclic surges of streaming are seen. These surges are associated with entrance of granular endoplasm into the hyaline cap region (this has been called sporadic streaming [Allen, 1973; Mast, 1926; Mast and Prosser, 1932]). In some cases surges and hyaline cap cycles are probably a trivial result of external perturbations and random fluctuations as a specimen moves, but in other instances they appear from their regularity to be autonomous oscillations. Although autonomous oscillations involving the hyaline cap do not occur for the calculation currently under discussion, they do occur for slightly different parameters (these results are complicated and will be discussed in a subsequent publication).

Grebecki (1984) has reported very extensive studies of the contraction of the ectoplasm of amoeba *A. proteus* when the organism is free of any adhesive contacts and also when the organism is adhering to the substrate at various points. The results confirm once again that full fountain flow is a phenomenon seen only in unattached amoebae and in amoebae attached to the substrate at the tail. Grebecki's results for unattached amoebae can be summarized by a simple rule: "All parts of the ectoplasmic tube in unattached amoebae undergo axial contraction at a uniform rate." Grebecki's rule may be cast in the more mathematical form:

$$-\partial_z V_z^{(n)} \approx \text{const},$$

for points lying in the ectoplasmic tube.

The value of the constant appearing in Grebecki's rule is called the ectoplasmic contraction rate. Based on the published data of Grebecki, this quantity has the value 0.015 s^{-1} in the typical monopodial *A. proteus* in the absence of adhesion. Yagi (1961) also studied the contraction rate of the ectoplasm but using a different technique and without taking sufficient pains to control adhesion. As a result Yagi did obtain some differences in the contraction rate in the anterior, middle, and posterior segments of the ectoplasmic tube. Nevertheless, Yagi's measurement of the contraction rate at the midpoint of the ectoplasmic tube (0.018 s^{-1}) agrees with Grebecki's result to within the standard deviation.

One can readily see from the linearity of the curve for network velocity in Fig. 4 *b* that the minimal model closely obeys Grebecki's rule. The parameters in Table 1 have been chosen so that the ectoplasmic contraction rate at the midpoint is in agreement with the data of Grebecki and Yagi. It is also seen from Fig. 4 *b* that the minimal model predicts a sudden dramatic increase in the network contraction rate at the anterior end of the ectoplasmic tube (i.e., at the point where the tube joins with the plasma gel sheet). This prediction is not contrary to Grebecki's rule because the rule only holds posterior of the plasma gel sheet.

At least superficially, it would seem that Grebecki's rule is contradictory to the observation of constant ectoplasmic composition reported by Allen and co-workers (see above). The minimal model is able to achieve consistency between these two observations only by invoking a very important role for the continual chemical assembly and disassembly of the network ($\mathcal{J}$). The importance of this chemical reaction can be understood best by considering the value of its time constant, τ_n = 12 s. In other words, an element of the polymerized cytoskeleton of *A. proteus* remains in this state for an average of only 12 s before being recycled into the soluble pool of precursors. In support of this rather remarkable prediction, one may cite the photobleaching studies of labeled actin in *A. proteus* (Wang et al., 1982). This study reported the virtual absence of a low mobility actin fraction corresponding to F-actin, despite the obvious presence of large amounts of labeled F-actin. This paradoxical result can be understood if the chemical equilibration of F and G is fast, compared to the time for diffusive mixing, since in this limit both F- and G-actin move as a single species.

The transverse shear rates of the network and/or solution are defined by the quantities $\partial_r V_z^{(n)}$ and $\partial_r V_z^{(n)}$, respectively. According to Allen, these quantities are negligible in the ectoplasm near the lateral boundary but not negligible in the endoplasm and possibly also at the boundary of the endoplasm and ectoplasm (Allen, 1973; Allen, 1961 *a* and *b*). This aspect of the fountain flow is usually interpreted as supporting the notion of a marked difference in the consistency of the endoplasm and ectoplasm. To demonstrate the predictions of the minimal model concerning these observations, Fig. 5, *a* and *b*, show plots of the z-component of velocity for solution and network versus the radial position, r. The axial locations in these figures are matched with those of Fig. 3: one near the posterior, one at the midpoint, and one at the anterior end of the endoplasmic channel. At all three locations. the z-velocity components are practically constant near the lateral boundary. The thickness of the low shear zone is

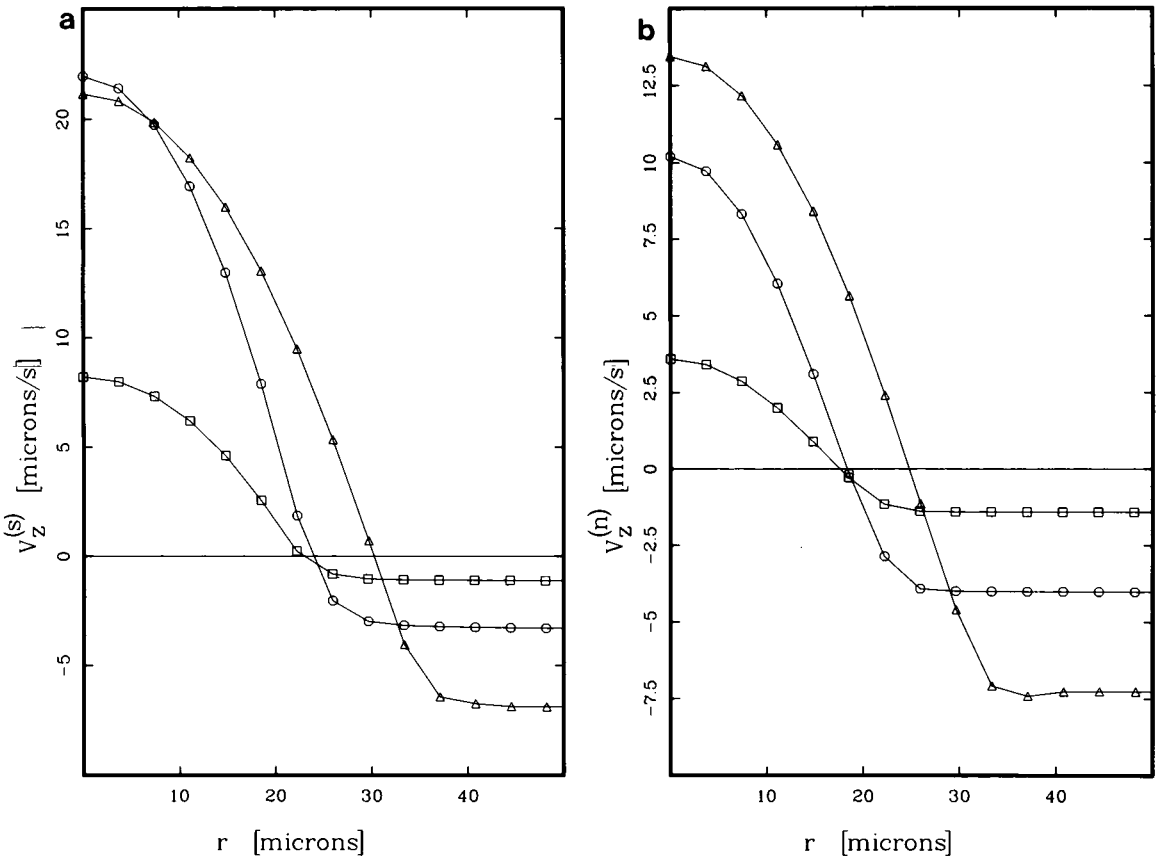

FIGURE 5 (*a*) $V_z^{(s)}$ versus r at three values of z. The predictions of the minimal model for the z-component of solution flow at the posterior (*squares*), middle (*circles*), and anterior (*triangles*) are shown. The values of z at these three cross-sections are matched with Fig. 3. In the fountain zone (anterior) the velocity of backward movement near the lateral boundary is approximately one third the velocity of forward flow near the axis (Allen's "velocity ratio" rule). For all three cross-sections there is a region of low traverse shear near the lateral boundary. This region is narrow near the anterior but increases in thickness near the posterior, in correlation with the thickness variation of the ectoplasm (see Fig. 3). (*b*) $V_z^{(n)}$ versus r at three values of z. The predictions of the minimal model for the z-component of network flow at the posterior (*squares*), middle (*circles*), and anterior (*trangles*) are shown. The values of z at these three cross-sections are matched with Fig. 3. The qualitative behavior of the network flow is similar to that of the solution (Fig. 4 *b*) and is at least superficially in accord with the prediction of the frontal contraction model. Contrary to the prediction of the frontal contraction model however, the forward flow of the network in the endoplasm is much slower than the forward flow of the solution (compare Fig. 4, *c* with *b*). Thus in the minimal model, the forward flow of network filaments in the endoplasm is driven by hydraulic drag of the solution phase and not vice versa. (*c*) Predicted and experimental velocity profiles in the endoplasm. Solid lines show the prediction of the minimal model for the flow profile of the solution phase at the anterior, posterior, and middle of the endoplasmic channel. These theoretical results are the same as in *a* except that velocities and radii have been normalized so as to remove differences due to variations of channel diameter and maximum speed. Also shown (*dashed line*) is the parabolic velocity profile predicted for Poiseuille flow. All the theoretical curves are virtually indistinguishable from each other. The data points show the velocity profile measurements of Allen and Roslansky (1959). Triangles give measurements at the posterior, closed circles at the middle, and crosses at the anterior of the endoplasmic channel. The data are consistent with a parabolic velocity profile at all three axial locations.

large at the posterior and small at the anterior, reflecting the underlying changes in the thickness of the ectoplasmic tube.

Allen et al. (1960) have reported a general rule of the fountain flow that may be stated as follows: the forward velocity of particles in the fountain zone near the center of the endoplasm is between two and three times faster than the velocity of particles retreating from the fountain zone in the ectoplasm. By examining the velocity profile for the anterior in Fig. 5 *a*, one may verify that the minimal-model is consistent with Allen's rule.

Fig. 5, *a* and *b*, indicate that there are considerable differences between anterior, posterior, and middle with respect to the maximum velocity of forward flow and also with respect to the diameter of the channel of forward moving material. To see if there are also differences in the detailed velocity profile of the forward flowing material, it is useful to replot curves such as those shown in Fig. 5 *a*

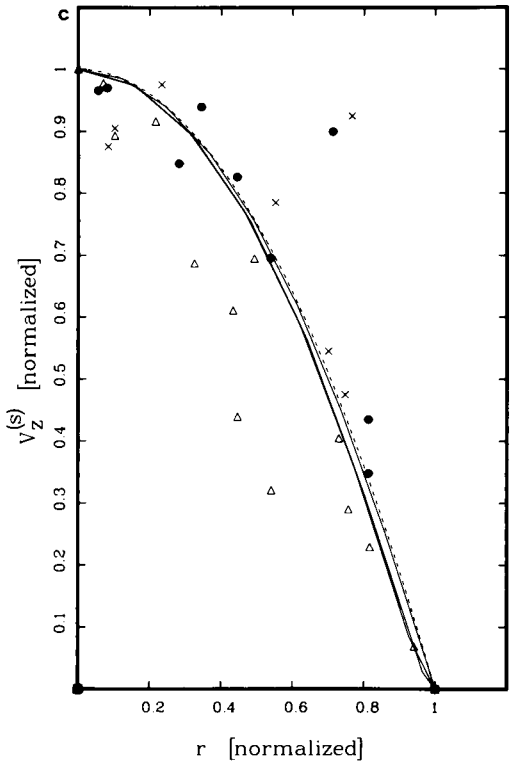

FIGURE 5 Continued

using nondimensionalized velocity and distance scales. To normalize the velocity, one naturally uses the maximum flow rate at the axis; and to normalize radius, one may use the value of the radius at which the velocity changes from positive to negative. When this is done, the velocity profiles at the anterior, posterior, and middle are always found to lie within 1% of the profile expected for simple Poiseulle flow (i.e., a parabola).

Fig. 5 *c* shows the universal parabolic velocity profile predicted by the minimal model for the forward flow of the solution phase of the endoplasm and compares the prediction with the measurements of Allen and Roslanski (1959). It is rather disappointing to note that a strong test of the theory is precluded by the considerable scatter of the data. For example, one may observe a slight tendency for the data collected at the posterior to lie below the predicted curve and for data collected at the midpoint and the anterior to lie above the predicted curve. Allen and Roslanski claimed that the indicated discrepancies were large enough to disprove the hypothesis of a parabolic velocity profile at the middle and the anterior portions of the flow, but the data clearly do not support this claim on an objective basis. It is our conclusion that the observed velocity profiles are close to being parabolic and are, therefore, consistent with the minimal model.

Fig. 6, *a* and *b*, shows the predictions of the minimal model for the radial components of network and solution motion at three different locations along the endoplasmic channel. The first thing to notice is that, except at the most anterior cross-section, the radial motions of the solution phase are directed toward the axis and that this component of motion is very slow compared with the axial flow. Thus tracer particles in the main part of the endoplasmic channel do not tend to migrate toward the lateral boundaries and, in fact, will experience a slight tendency to migrate toward the axis. This is necessary if the model is to account for complete stability of particle trajectories in the central part of the endoplasmic channel.

Boundary conditions

Several of the boundary conditions employed by the minimal model can be directly checked experimentally. Most importantly, the minimal model postulates that the plasma membrane remains stationary and is able to slide freely with respect to the ectoplasmic tube. This assumption has been directly verified many times by observing the behavior of small particles or fluorescent labels on the exterior of the plasma membrane (Mast, 1926; Griffin and Allen, 1960; Grebecki, 1987). The fact that the cytoskeleton is able to slide over the membrane while at the same time adhering to the membrane implies an extremely fluid coupling mechanism.

The minimal model also postulates that the network phase is poorly anchored to the plasma membrane at the anterior surface of monopodial *A. proteus*. Remarkably, random detachment of "waves" of network from the inner surface of the plasma membrane at the anterior surface can be directly visualized in specimens of *A. proteus* microinjected with fluorescenated actin (Taylor et al., 1980*b*). This material is seen to flow inward through the hyaline cap and to be incorporated into the plasma gel sheet just as expected. In contradiction of the experiments, however, the minimal model predicts that detachment of the network from the anterior membrane will be a smooth continuous process whereas the actual event seems to be periodic. It may be that this indicates a fundamental limitation of continuum mechanics in describing such small amounts of matter. More likely, however, the no-stick boundary condition is an oversimplification of the real situation at the anterior surface. In other words, adhesion of the network to the anterior may be much weakened but not completely absent.

Calcium

The minimal model assumes that cybernetic factor equals calcium and that calcium controls the network contractility in amoebae according to a simple linear constitutive

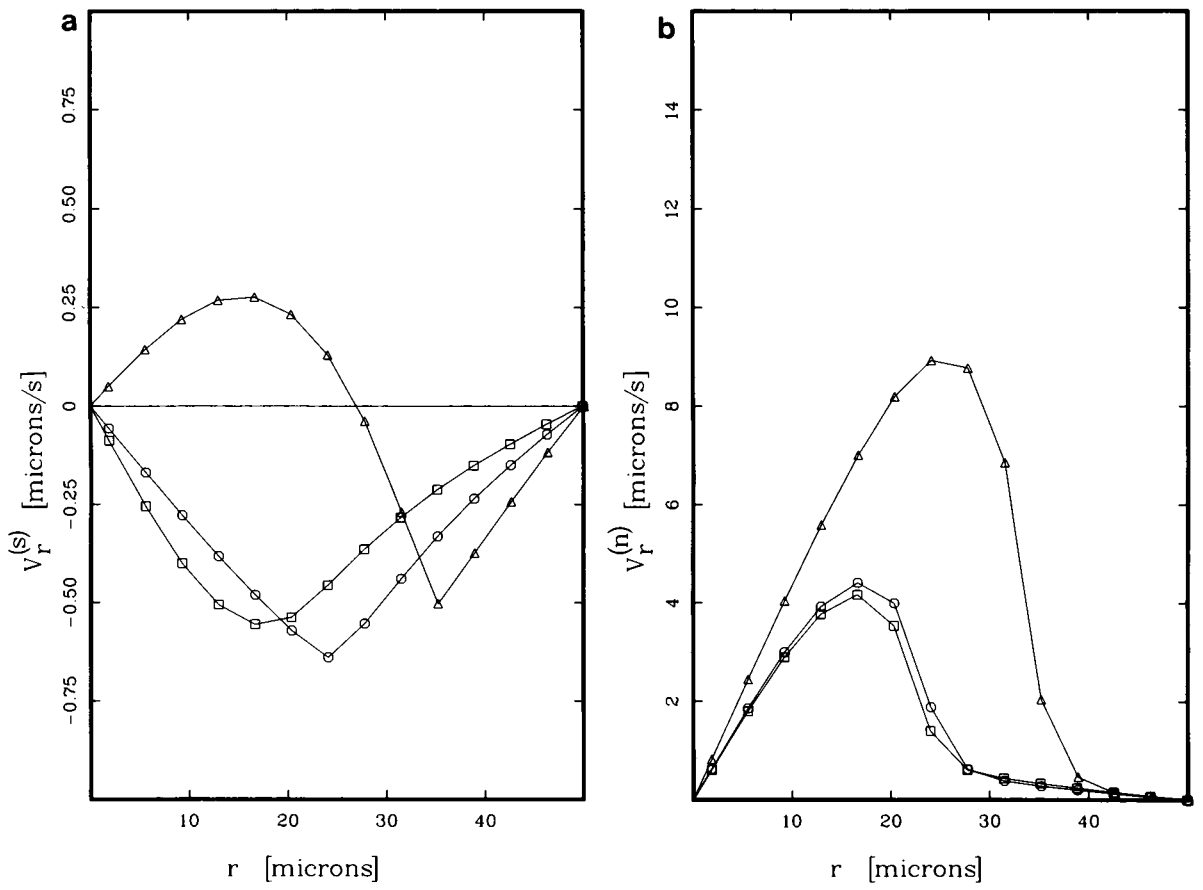

FIGURE 6 (*a*) $V_r^{(s)}$ versus r at three values of z. The predictions of the minimal model for the r-component of network flow at the posterior (*squares*), middle (*circles*), and anterior (*triangles*) are shown. The values of z at these three cross-sections are matched with Fig. 3. The main conclusion is that there is a slow lateral motion of the solution phase towards the axis until very close to the anterior opening of the ectoplasmic tube. (*b*) $V_r^{(n)}$ versus r at three values of z. The model requires that there be a considerable component of lateral motion of the network phase even within the endoplasmic channel.

law. The evidence for this comes largely from the in vitro studies of Taylor and co-workers and is reasonably compelling (Taylor et al., 1973). The diffusion constant of the cybernetic factor and the threshold for contraction (Table 1) follow directly from these studies (see preceding section). In order to encode spatial information, the characteristic lifetime of the cybernetic factor must be approximately equal to the time required for diffusion of the factor over a distance on the order of the spatial distance encoded. For the case at hand the spatial distance encoded is the characteristic distance separating endoplasm from ectoplasm, or $\approx 0.5\ r_0$. This simple consideration sets upper and lower limits on τ_q that are sufficient to determine the value indicated in Table 1. If τ_q is much larger than the indicated value, then contraction in the endoplasm becomes too strong and regions of ectoplasm form at the axis. If τ_q is much shorter than the indicated value, then there is insufficient contraction in the endoplasm; the density of filaments in the endoplasm becomes too high, the boundary between endoplasm and ectoplasm is too blurred, and a plasma gel sheet fails to assemble.

According to Fig. 2, calcium should be distributed diffusely throughout the length of the amoeba without significant anterior-posterior gradient.[2] The minimal model also predicts a cortico-medullary gradient of calcium (i.e., that calcium is maximum at the plasma membrane and minimal at the center of the amoeba). It can be seen from Fig. 2, however, that the calcium concentration never actually goes below the contraction threshold. This implies that the difference in network contractility in ectoplasm versus endoplasm is close to the difference between "flair" and "relaxation" solutions (Taylor et al., 1973) but that even in the endoplasm there is still some tendency to contract. It also implies the

[2]There is a slight anterior-posterior gradient of cybernetic factor caused by convective transport, but this is quite insignificant.

existence of a sink for calcium in the interior of the cytoplasm and a source of calcium at the membrane.

The observed distribution of calcium, based on Aequorin luminescence, does indicate significant calcium levels throughout the cell, but there was no report of a corticomedullary gradient; and in contradiction of the minimal model, maximum calcium concentrations occurred at the tail (Taylor et al., 1980*a*). These discrepancies suggest that the assumptions of the minimal model are too simplified with regard to the dynamics of the cybernetic factor and/or with regard to the nature of the coupling between the cybernetic factor and the cytoskeleton (cf. Discussion).

Consistency

Yagi (1961) has reported measurements of the viscosity near the axis of the endoplasmic stream of amoeba *A. proteus* using carefully calibrated magnetic particles between 2 and 9 μm in diameter. These experiments are technically difficult for many reasons (for one thing, the viscosity tends to decrease with successive measurements). Nevertheless, the average result for 33 measurements on three specimens was that the endoplasm behaves like a viscous fluid with viscosity of 0.9 poise (SD ± 0.6 poise). Data in good quantitative agreement with Yagi's result have recently been obtained by Sato and Allen (1983) in the endoplasm of *Physarum polycephalum*. Because both the biological material and the experimental difficulties associated with these two studies were quite different, the agreement greatly encourages one to take the results seriously.

As we have discussed previously (Dembo and Harlow, 1986), the viscosity reported by the magnetic particle technique corresponds to the volumetric average of the microscopic network and solution viscosities. Because the contribution of the solution viscosity to this average is negligible in the present case, Yagi's experiment in effect yields a local value for the product of the network volume fraction and the specific network viscosity: $f\mathcal{M} = f\mu_n \exp[(f/\rho_{gel})^2]$. From Fig. 3 *a* we see that $f \approx 7 \times 10^{-4} \ll \rho_{gel}$ in the endoplasm. Combining this result with the viscosity measurement yields the value of μ_n given in Table 1.

From the computed density of network in the ectoplasm and the parameters in Table 1, the minimal model predicts the macroscopic viscosity of the ectoplasm to be ~3,000 poise! Materials of similar viscosity in common experience are window glass and road asphalt (on a cold day). The huge difference in viscosity between endoplasm and ectoplasm occurs partly because the density of network in the ectoplasm is larger and partly because the specific viscosity of the network is increased by gelation. In any event, if one approximates the amoeba as a lump of viscoelastic material, then the effective properties of this material should be completely dominated by the contribution of the ectoplasm.

Yagi (1961) attempted to directly determine the macroscopic viscosity of the ectoplasm, but unfortunately the value was too large to be measured by his magnetic particle technique. More recently the rheology of cytoplasm of granulocytes has been measured by observing the deformation and recovery of the cell as a whole using the micropipette aspiration technique (Evans and Kukan, 1984; Dong et al., 1988). When such data are fitted to the model of a Maxwell fluid with constant surface tension, viscosities on the order of 300 poise and time constants for Maxwellian relaxation on the order of 1 s have been obtained (Dong, et al., 1988). Whereas these data may not be quantitatively relevant to *A. proteus,* they at least show that huge viscosities on the order predicted by the minimal model are possible and can be measured. They also indicate that the elastic component of the network compliance is negligible in comparison to viscosity. It is worth mentioning that Yagi also observed some amount of elastic recoil in his compliance tests of the ectoplasm (though not in the endoplasm).

Pressure gradients

One of the most interesting aspects of Fig. 2 is the predicted (relative) pressure field inside the monotactic amoeba. For example, the calculation predicts that the pressure gradient driving the flow of the endoplasm (also called the "motive force") is fairly constant along most of the endoplasmic channel. The pressure gradient is about 1.4×10^3 dyn/cm^3 if one takes a reading near the midpoint. To measure the motive force experimentally entails the artificial production of a countervailing pressure gradient in the amoeba so as to exactly cancel the forward streaming of the endoplasm. The countervailing pressure gradient must be applied as a short burst so as to avoid any irreversible physiological complications produced by sustained stoppage of normal streaming. As a control it is important to ensure that normal streaming is resumed as soon as the countervailing pressure gradient is removed.

To produce the countervailing pressure gradient, it is necessary to apply hydrostatic pressure to the anterior end of the amoeba by placing a micropipette over the hyaline cap while at the same time holding constant the pressure at the posterior end of the amoeba. It is the latter requirement that produces difficulties. To overcome these difficulties Allen and Roslansky (1959) made use of the large highly polypodial form of *Chaos carolinensis*.

The advantage of the polypodial form is that many pseudopods emerge from a central body, like the tubes on a bagpipe. To a first approximation each pseudopod can be thought of as a monopodial amoeba that is joined to

other amoebae at the tail. It thus was hoped that pressure could be applied to reverse the fountain streaming in one of the pseudopods while the remaining pseudopods would act as "relief valves" to effectively buffer the pressure in the central body. In any event if one assumes that the pressure in the body remained constant, then the pressure gradient required to halt streaming in a single pseudopod can be calculated and was found to be 5.6×10^3 dyn/cm^3. If the pressure in the central body was not well buffered, then this represents an overestimate of the pressure gradient required to reverse streaming.

In support of the validity of the approach taken by Allen and Roslansky, it should be mentioned that Rinaldi et al. (1975) repeated their experiment and obtained essential agreement. Finally, it is interesting that the pressure gradients measured by Allen and Roslansky are of the same magnitude as the pressure gradients that drive endoplasmic streaming in *Physarum polycephalum*. These latter are measured by the "double chamber" technique (Kamiya and Kuroda, 1958; Kamiya, 1959).

The pressure gradient measured by Allen and Roslansky (1959) is some threefold higher than the gradient predicted by the minimal model. At present, we feel that this is an acceptable discrepancy because the uncontrolled factors in the experiments tend to inflate the measured gradients relative to theory. In general, one can only reject models that predict pressure gradients significantly higher than the value measured by Allen and Roslansky.

Heat and work

Take the dot product of Eq. 3d with the vector $V_i^{(n)}$. After making some simple rearrangements based on the chain rule, the result can be expressed as follows:

$$\partial_{x_j}[f\mathcal{M}V_i^{(n)}E_{ij}^{(n)}] + \partial_{x_i}[f\mathcal{C}V_i^{(n)}] + 0.5f\mathcal{H}[V_i^{(s)} - V_i^{(n)}][V_i^{(s)} + V_i^{(n)}] = 0.5[f\mathcal{M}E_{ij}^{(n)}E_{ij}^{(n)}] + 0.5f\mathcal{H}[V_i^{(s)} - V_i^{(n)}]^2 + 0.5[f\mathcal{C}E_{jj}^{(n)}]. \quad (7)$$

This expression is nothing else but the equation of kinetic energy balance for the network phase (in the creeping flow limit). If we consider a small control volume, then the three terms on the left are easily interpreted in the usual way. They are the boundary workings due to viscous stresses in surrounding network material, the boundary workings due to contractile stresses in surrounding network material, and the interphase working on the network by the drag of the solution phase. On the right we have the heat dissipated inside the control volume due to viscosity of the network: one half of the heat dissipated inside the control volume due to interphase drag and the work done inside the control volume against the contractile stresses of the network. One could, of course, go on to obtain a full energy equation by adding terms for the diffusion and convection of heat through the boundaries of the control volume and between the phases, the loss of chemical potential energy, etc. We will not bother with these embellishments.

We can obtain the equation for balance of kinetic energy in the solution phase by a completely analogous procedure. After applying the conservation of volume, the result takes the form

$$\partial_{x_j}[\mu_s V_i^{(s)}E_{ij}^{(s)}] - \partial_{x_i}[pV_i^{(s)}] + 0.5f\mathcal{H}[V_i^{(n)} - V_i^{(s)}][V_i^{(s)} + V_i^{(n)}] = 0.5[\mu_s E_{ij}^{(s)}E_{ij}^{(s)}] + 0.5f\mathcal{H}[V_i^{(s)} - V_i^{(n)}]^2 \quad (8)$$

The terms on the left are the boundary workings due to the solution viscosity and pressure and the interphase working on the solution. The terms on the right are the heat dissipated inside the control volume by solution viscosity and the (other) half of the heat dissipated at the interface between the solution and the network.

Fig. 7 graphically illustrates the exact spatial distribution of the sources and sinks of kinetic energy during steady fountain flow according to the minimal model. The top three panels are color contour plots showing the rate at which energy is being dissipated as heat at different locations due to solution viscosity, interfacial drag, and network viscosity. The last panel shows the opposite side of the ledger, namely, the power being supplied by network contraction at various locations.

From the lowest panel in Fig. 7 one notes the curious fact that the power supply is negative in certain parts of the cytoplasm (notably the endoplasmic channel). As can be directly inferred from Eq. 7, this occurs when the local flow field is such that it causes a dilation or stretching of the network filaments. At such locations power is absorbed because the contractile efforts of distant filaments are being used to work against and overcome the contractile tendency of the local filaments. In an inefficient system the power used in this struggle could be wasted and appear as heat, but this does not have to be if the dilated filaments can temporally store the energy supplied by the distant filaments and redeliver it when they themselves have moved to the distant location. In the minimal model the power requirement and heat production assume that the contractile machinery is sufficiently clever to utilize the latter scheme. If the former scheme is assumed, then power requirements are increased by ~10%.

Another interesting fact about the last panel of Fig. 7 is the extraordinarily high rate at which energy is being delivered to the small region at the very tip of the ectoplasmic tube (the magenta spot). One can get some idea of the importance of the magenta spot from the fact that by itself (without including any of the red or orange zones nearby) it accounts for 35% of the total work done

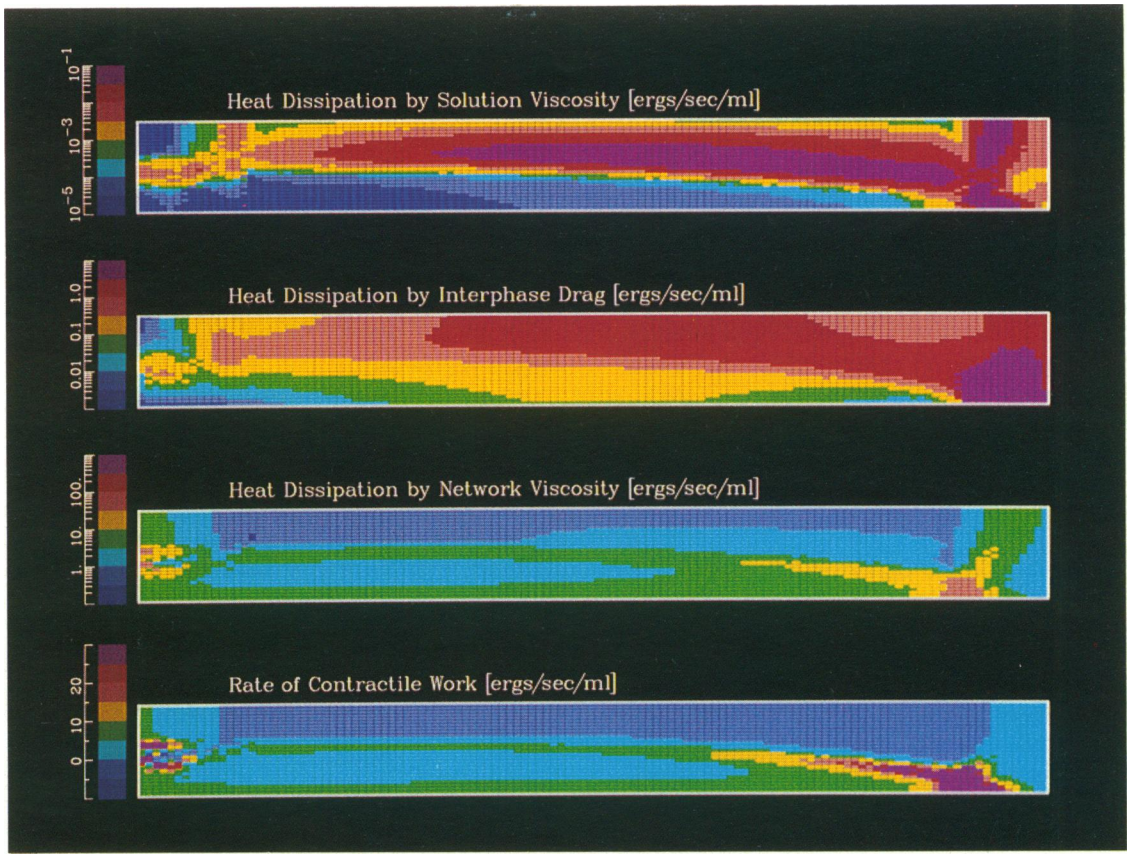

FIGURE 7 Spatial distribution of work and heat. Shown are false color contour maps of the rate at which mechanical work is being done by the cytoskeleton, the rate at which heat is being generated due to network viscosity, the rate at which heat is being generated due to interphase drag, and the rate at which heat is being generated due to solution viscosity. Color scales appear to the left of each subplot. The integrated power supply is 2.35×10^{-5} ergs/s per cell; the integrated loss due to network viscosity is 2.00×10^{-5} ergs/s per cell; the integrated loss due to interphase drag is 0.34×10^{-5} ergs/s per cell; and the integrated heat loss due to solution viscosity is 0.005×10^{-5} ergs/s per cell. About 35% of the power supply is derived from the magenta-colored region in the lower contour map, with the rest being delivered uniformly throughout the ectoplasmic tube. The magenta spot coincides with the point of maximum tactile- and photo-sensitivity of the amoeba (see text).

by the cytoskeleton in driving the fountain flow. The rest of the power required by the fountain flow is delivered more or less uniformly throughout the ectoplasmic tube. The really surprising thing about the magenta spot is not simply the fact that such a compact and intense energy source is predicted by the minimal model but the fact that it is located near the front of the cell and not at the tail.

Despite many points of disagreement between Allen's frontal contraction model (Allen, 1961*a*) and the minimal model, in some respects the minimal model owes a great deal to Allen's ideas. For example, models based purely on contraction of the ectoplasmic tube have always been at difficulties to explain the evidence for considerable network structure and contractility in the endoplasm. Furthermore, these models do not give a very satisfactory account of the photo and tactile sensitivity of pseudopod tips. We do not think it is coincidental that the magenta spot occurs precisely at the point of maximum response of the amoeba to localized stimulation (Allen, 1961*b*).

Suppose that we add Eqs. 7 and 8 and integrate the result over the interior of the region Ω. We find that all the terms on the left side either cancel or vanish when we apply the divergence theorem and the boundary conditions. On the right we have the sum of four terms: the total power supplied by network contraction, the total power lost as heat due to the network viscosity, interphase drag, and solution viscosity, respectively. Thus in the minimal model of fountain flow, all the work done by the contractile machinery of the cell is immediately dissipated as heat. This is a consequence of our assumption of creeping flow and our assumption that the region Ω has fixed boundaries. The former assumption implies that kinetic energy is rapidly dissipated as either heat or work, and the latter assumption prevents the amoeba as a whole

from doing useful work on its surroundings. Incidentally, the existence of a global energy balance is very useful for debugging computer codes and checking their accuracy.

In the minimal model, the total rate at which the contractile apparatus does mechanical work (i.e., the integral of the quantity $-0.5\,fCE_{jj}^{(n)}$) is 2.35×10^{-5} ergs/s per cell. Of this amount 2.00×10^{-5} ergs/s per cell is converted to heat due to network viscosity; 0.34×10^{-5} ergs/s per cell is converted to heat by interphase drag; and a very small amount, $\approx 0.005 \times 10^{-5}$ ergs/s per cell, is converted to heat by solution viscosity. These sources of heat represent only the direct results of contractile activity. Reference to a textbook of physiology (Astrand and Rodahl, 1986) will show that only ~20% of the energy released by oxidation of glucose can actually be converted to work by contractile systems. Thus in addition to the heat generated as a direct result of contractile activity, $\sim 9.4 \times 10^{-5}$ ergs/s per cell is generated as an indirect result.

It is well known that one molecule of ATP must be hydrolyzed each time a molecule of actin cycles between the polymerized and the depolymerized forms. Thus, in addition to heat generated as a direct or indirect consequence of contractile activity, some heat is generated as a result of purely chemical processes in the minimal model. Knowing the turnover time of the cytoskeleton, τ_n, and the average density of the cytoskeleton, ρ_{ceq}, one may easily calculate that actin polymerization in the minimal model requires $\sim 3 \times 10^{-17}$ mol of ATP/s per cell. The heat liberated directly and indirectly due to the hydrolysis of this much ATP is $\sim 2.5 \times 10^{-5}$ ergs/s per cell. Thus the heat liberated due to the continual chemical assembly and disassembly of the cytoskeleton is ~25% of the heat that results from contractile activity.

If one adds everything up, the minimal model predicts that the total heat generated both directly and indirectly as a result of the mechanical and chemical activity of the cytoskeleton is $\sim 1.2 \times 10^{-4}$ ergs/s per cell. There might seem to be little hope of ever obtaining evidence relevant to this prediction, but, in fact, Nassberger and Monti (1984) have made rather precise measurements of the rate of energy utilization by *A. proteus* using the technique of microcalorimetry. At very low cell densities they obtain a steady value of 1.4×10^{-2} ergs/s per cell after 3 d of starvation. Obviously, if the minimal model is correct, then these data imply that the whole phenomenon of fountain flow is nothing but a drop in the bucket as far as the overall energy budget of the *A. proteus* is concerned.

A complementary approach to estimation of the energy flux in fountain flow is provided by studies of the behavior of *A. proteus* in the centrifuge microscope (Allen, 1960). From such studies it was shown that an amoeba can do sustained mechanical work on the exterior at a rate of at least 1.3×10^{-6} ergs/s per cell. According to the minimal model, this rate of sustained work is ~5–6% of the total power output of the cytoskeleton and is thus quite feasible. In fact, if the minimal model is correct, we would expect amoeba to be able to do at least two or three times better than this. It may be that the conditions of Allen's experiments were not quite optimal for the performance of work. Alternatively, the amoebae in Allen's experiments may not have been sufficiently "motivated" to perform maximum work against the centrifugal field. To provide such motivation, perhaps the chemotactic or photophobic sensitivities of amoebae could be put to good use.

Boundary stress

Let us for the moment make the simplest possible conjecture concerning the mechanical properties of the surface layer of *A. proteus*, namely that the surface behaves like a simple liquid–liquid interface or a soap film. This means that bending rigidity and surface viscosity are negligible and that the layer possesses a surface tension that is a constant independent of its state of deformation or motion.

If N_j are the components of the outward directed normal vector at some point on the surface, then the balance of normal stresses can be stated as follows:

$$\{-\mathcal{M} f N_j E_{ij}^{(n)}\} + \{-\mu_s N_j E_{ij}^{(s)}\} + \{-\mathcal{C} f N_i\} + \{pN_i\} = [2\gamma \bar{C} - p_0]N_i. \quad (9)$$

On the left of this equation are four terms enclosed in { }. These represent the outward normal stresses due to network viscosity, solution viscosity, network contraction, and relative pressure, respectively. On the right of the equation are the inward normal stresses due to surface tension, γ, and turgor pressure, p_0. One should recall our previous discussion (see sections on microanatomy and boundary conditions) for the definitions of the turgor pressure and of the mean curvature, $\bar{C}$.

An important aspect of the logic of Eq. 9 is the implicit assumption that the surface layer of *A. proteus* is two-dimensional and in some sense "smooth." It is well known that the actual surface layer is quite thick and consists not only of the lipid bilayer but the glycocalyx and a support structure of membrane-associated proteins. Moreover, the surface layer contains many microscopic ruffles and foldings, especially at the uropod. Given these realities, how can one talk of surface tension or even define a mean curvature? The answer is that a smooth surface can approximate a surface that is corrugated on a micron scale just as well as one that is corrugated on a molecular scale if the spatial wavelengths of interest are large compared with microns. It remains to be seen if such a continuum approximation can work in the case of the

surface of *A. proteus* because one is much closer to the limit of its validity than is usually the case.

Fig. 8 *a* shows the values of the four individual terms on the left-hand side of Eq. 9, according to the numerical solution of the minimal model. All four terms are shown in absolute value in order that they can be displayed on the same scale, but it should be remembered that the contractile stress pulls "inward" and the other three stresses push "outward." Fig. 8 *b* shows the result when we subtract the contractile stress from the sum of the other three stresses.

According to Eq. 9, the normal stress on the boundary of an amoeba is related to the mean curvature of the boundary by a simple linear transformation. As a rough test of this prediction one may compare the shapes of the curves in Figs. 8 *b* and 1 *b*. The two are obviously very close, the main discrepancy being that the outward stress goes through a relative minimum near the middle of the endoplasmic channel whereas the minimum of mean curvature occurs just before the hyaline cap.

To conduct an exact test of Eq. 9, the boundary stresses should be computed for a domain with the exact shape of the amoeba as given in Fig. 1 *a*. Use of the cylindrical region Ω yields only an approximation to the true boundary stresses, and the nature of this approximation may well account for the discrepancy between Figs. 1 *b* and 8 *b*. One is therefore tempted to try different simple shapes for the amoeba to see if this approximation can be improved. Accordingly, we have carried out a series of computations using truncated cones with various angles of taper as models of the amoeba. If the angle of taper is chosen optimally, one can get much improved agreement between the calculated boundary stress and the mean curvature, but there is still some discrepancy that cannot be removed. These results provide even stronger circumstantial evidence for the validity of Eq. 9 and for the underlying conjecture about the mechanical properties of the surface layer of *A. proteus*. Nevertheless, in the final analysis the only way to establish the validity of Eq. 9 is within the context of a complete and internally consistent formulation of the free boundary problem of cell motion (see below).

The additive and multiplicative constants of the linear relation connecting Figs. 1 *b* and 8 *b* yield the values of the turgor pressure and the surface tension of *A. proteus*, respectively (see Eq. 9). These constants can be adjusted until one obtains the best fit between Figs. 1 *b* and 8 *b*. Thus in an indirect way the minimal model in conjunction with Eq. 9 makes two rather remarkable and quantitative predictions: $\gamma \approx 0.10$ dyn/cm and $p_0 \approx 39$ dyn/cm^2. In view of the cumulative effects of the uncertainties of the parameters of Table 1 and of the fitting procedure, these predictions could easily be in error by a factor of two or three. Even with this large uncertainty, γ and p_0 represent extremely small values of surface tension and turgor pressure; for comparison the surface tension between olive oil and water is ~20 dyn/cm; the equilibrium turgor pressure produced by a transmembrane concentration jump of 1 μM of an ideal nonelectrolyte is ~25 dyn/cm^2.

At the present time there are no quantitative experimental measurements against which to test the predictions of the minimal model concerning γ and p_0. However, there seems no insurmountable obstacle to prevent the surface tension and/or turgor pressure of *A. proteus* from being measured experimentally, and there are at least some qualitative experiments that demonstrate the existence and significance of these quantities. For example, if the plasma membrane of *A. proteus* is mechanically ruptured at any point, then the initial reaction of the cytoplasm is to squirt outward (Grebecka, 1981). Czarska and Grebecki (1966) have discussed much evidence in support of their concept of the plasma membrane as a contractile surface carpet that tends to reversibly fold and unfold as the amoeba moves. Unfortunately they did not actually measure a surface tension of the carpet. Evans and Kukan (1984) have independently arrived at a very similar concept of the surface layer of granulocytes based on micromechanical studies. These latter authors did estimate the tension of the surface layer of the granulocyte and obtained a value of ~0.01 dyn/cm. Dong et al. (1988) obtained a value of 0.035 dyn/cm for the surface tension of granulocytes. These values are significantly smaller than the surface tension we predict for the amoeba. Hiramoto (1978) has reported measurements of the surface tension of the sea urchin egg ($\approx$0.15 dyn/cm) that are very close to the values we predict for *A. proteus*.

The basis of our analysis of fountain flow has been the ability to precisely formulate and numerically solve a certain class of models. The major limitation on this ability is the need to restrict consideration to fixed spatial domains of simple geometry. Because of the special properties of fountain flow, this restriction was not insurmountable, but for the most important and interesting phenomena of amoeboid motility (e.g., cytokinesis, phagocytosis, pseudopodal extension), the motion of the cell boundary is of the essence. Thus from the point of view of future theoretical directions, the most exciting consequence of the present results is that they suggest an extremely promising (but still hypothetical) continuum formulation of what may be called the full free boundary problem of cell motion.

If the plasma membrane is impermeable to fluxes of solution, then at a free surface the normal component of solution velocity is identical with the corresponding projection of the boundary velocity. This means that Eq. 4c no longer holds at a free boundary and that a new boundary condition is necessary. This new boundary

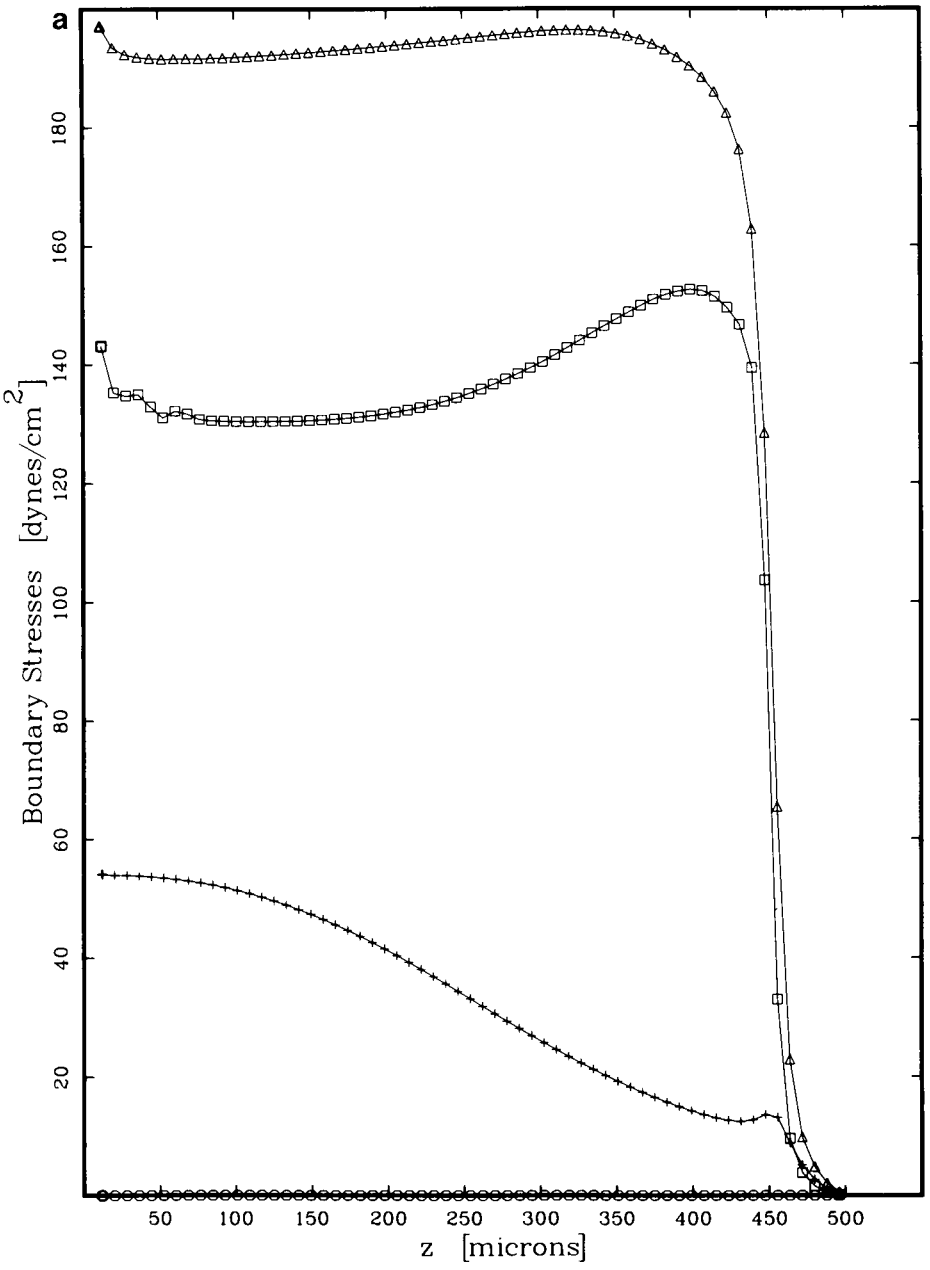

FIGURE 8 (*a*) Components of the boundary stress in the minimal model. The predictions of the minimal model for the four individual components of normal stress on the lateral boundary are shown as a function of axial position, *z*. The components are: the contractile stress (*triangles*), the viscous stress due to the network (*squares*), the viscous stress due to the solution (*circles*), and the pressure (*crosses*). All stresses are shown in absolute value, however, it should be remembered that the contractile stress pulls inward whereas the other three stresses push outward on the membrane. Also notice that the stress exerted by the solution is completely negligible on the scale of the other stresses. (*b*) Net boundary stress for the minimal model. The total normal stress on the lateral boundary is computed by subtracting the contractile stress from the sum of the other three stresses shown in the preceding figure. Thus positive values of the stress represent an outward force on the membrane. Comparison of the net normal stress with the mean curvature (see Fig. 1 *b*) reveals a definite correlation of the two quantities. This supports the validity of Eq. 9.

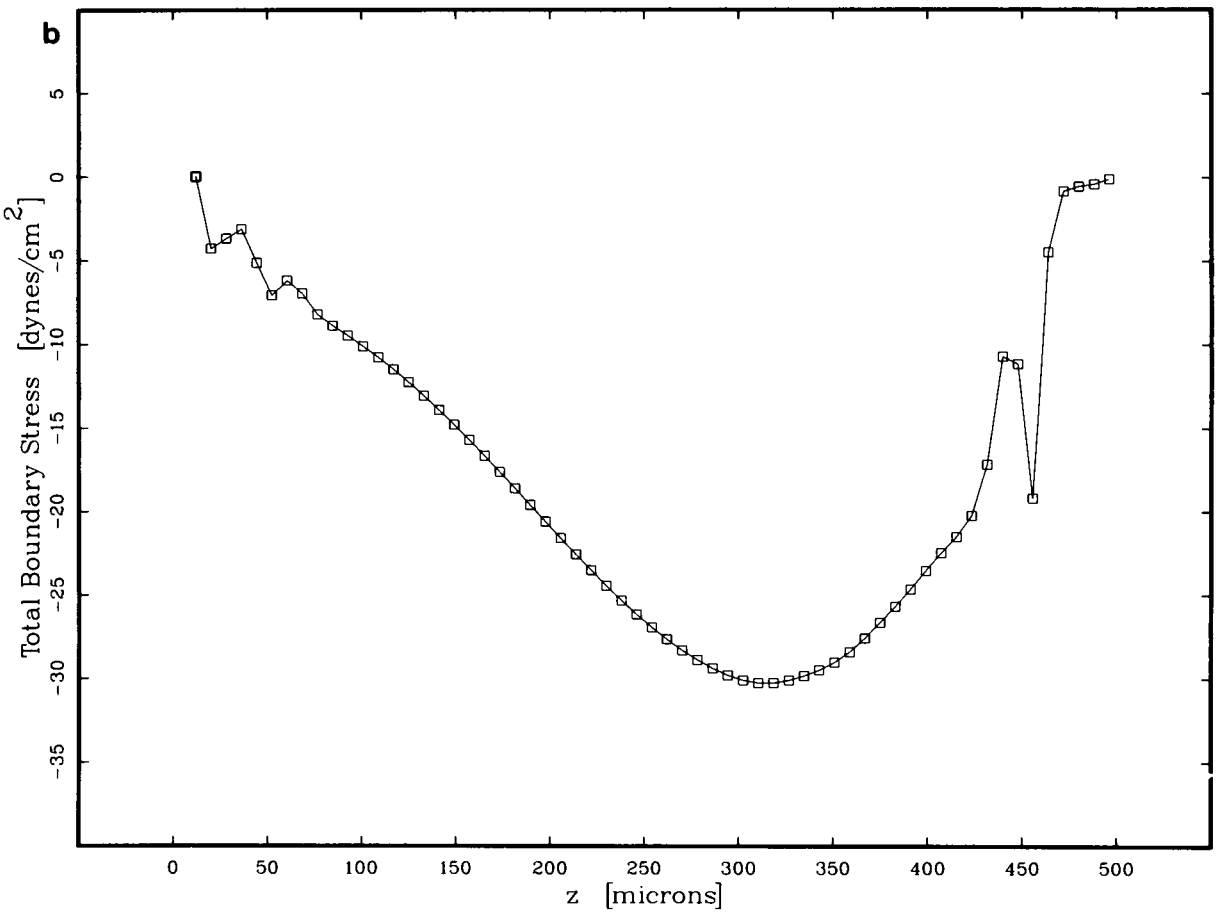

FIGURE 8 Continued

condition is provided by Eq. 9, the balance of normal stresses. The other conditions that describe a "free" surface are directly analogous to conditions that hold at fixed boundaries. First of all, because transverse momentum cannot be transported across a free surface, such boundaries should satisfy the slip condition, Eq. 4a, with no modification. The analogue of the stick condition (Eq. 4d) at a free surface is:

$$[V_j^{(n)} - V_j^{(s)}]N_j = 0. \tag{10}$$

If a free segment of the plasma membrane is no-stick, then Eq. 4e continues to hold, but the constraint condition is replaced by $[V_j^{(n)} - V_j^{(s)}]N_j \leq 0.0$ Finally, the Dirichlet and Neumann conditions on q at a free surface are the same as for the case of a fixed boundary (see Eqs. 4f and 4g).

DISCUSSION

The preceding presentation of the minimal model, the analysis of the model, and the comparison of the model predictions with data has been a fairly orderly and logical affair. In itself this is an exercise of limited utility; much more useful is to understand the biological issues involved in the "derivation" of the minimal model: why some models fail and why others work. This leads one to an exploration of the hypothesis space of which the minimal model is but a rather insignificant element. Unfortunately the journey through hypothesis space is not logical or deductive in nature; there are no rules, and it proceeds largely from generalization of empirical lessons learned from special cases.

A good place to start is with the distinction between endoplasm and ectoplasm. One wishes to explain the ability of the cytoskeleton to automatically organize itself into sharply delineated zones of high and low network density. After much empirical experience with the theory of reactive interpenetrating flow, we have found only two truly distinct dynamical mechanisms that are capable of doing this. These may be termed the $\mathcal{C}$-limit mechanism and the $\mathcal{M}$-limit mechanism.

The $\mathcal{C}$-limit mechanism postulates that if the network density gets too high, then other forces will dominate the

contractile tendency. In terms of the statement of a constitutive law, this implies that $\mathscr{C}$ is positive if f is close to zero but eventually declines and becomes negative as f gets large. Such a constitutive law for $\mathscr{C}$ is eminently reasonable because it seems quite obvious that contraction cannot go on forever and that at some point some sort of effective repulsive interactions between the network elements (e.g., competition for solvent) will become important.

The $\mathscr{M}$-limit mechanism postulates that the specific viscosity of the network phase, $\mathscr{M}$, is an increasing function of the network density. The form of this function must be such that $\mathscr{M}$ remains fairly constant at low values of f but that at some point $\mathscr{M}$ undergoes an explosive increase corresponding to the incipient gelation of the network. Such a transition of the network from sol to gel is quite distinct from the transition of network elements between disassembled (or monomeric) and assembled (or polymeric) states. A typical example of a constitutive law for gelation is used in the minimal model (Eq. 6c). We should note that we have also tried several other constitutive laws for describing gelation. Those that work well are characterized by an abrupt and unbounded rise of viscosity after a certain point and relatively little rise before this point; if the rise in viscosity is too gradual then the delineation between endoplasm and ectoplasm becomes blurred.

Both the $\mathscr{C}$-limit mechanism and the $\mathscr{M}$-limit mechanism cause the spontaneous assembly of regions of endoplasm and ectoplasm by imposing a kind of "fuzzy" upper bound on the extent to which the network phase can contract. If this bound is approached in some small domain, the contraction within the domain dramatically slows. At the same time contractions at the boundaries of the domain do not slow and continue to draw in additional network material so that there is a tendency for the domain to grow by accretion. This ultimately causes the formation of an appreciable region of ectoplasm. Unless some other factors operate (see below), the growth of ectoplasmic domains will ultimately stop only because of depletion of the network in the surrounding regions. Any regions not incorporated into the ectoplasm at steady state are by default endoplasm.

Despite a reasonable basis, we have been unable to account for the observed dynamics of the cytoskeleton of *A. proteus* using any model based solely on the $\mathscr{C}$-limit mechanism. Although such models produce distinct regions of endoplasm and ectoplasm, they do so by limiting the ability of network filaments in the ectoplasmic regions to develop stress. This means that the only filaments capable of contracting and doing extensive work are the filaments present in areas of low density, i.e., the filaments in the endoplasm and at the boundary between endoplasm and ectoplasm. At least in our hands, these few filaments are simply not capable of causing the ectoplasm to contract in such a way as to satisfy Grebecki's rule. There are also other difficulties with these models that are of lesser generality.

In a previous publication we have applied the general concepts of reactive interpenetrating flow theory to the dynamics of dissociated cytoplasm (Dembo, 1986). The model proposed at that time worked fairly well as far as the limited data concerning dissociated cytoplasm was concerned. Unfortunately for us, when we proceeded to apply this early model to the case of intact amoeba, it failed rather decisively. In retrospect we can see that the main problem with the early model was that it attempted to account for the endoplasm-ectoplasm dichotomy by means of a $\mathscr{C}$-limit mechanism.

The processes of contraction and gelation cause the removal of network material from the endoplasm and the accumulation of this material in the ectoplasm, but this is not enough to explain the continuous or cyclical nature of fountain flow. To obtain a closed loop of material flux, we require a steady replenishment of network in the endoplasm and the steady removal of network from the ectoplasm. All previous models of the fountain flow with which we are familiar employ what may be called the "reversal" mechanism to effect this replenishment. This means that in some region near the tail end of the cell (usually called the recruitment zone) the process of limited contraction that caused the formation of ectoplasm from endoplasm in the first place is simply reversed. Obviously, this mechanism requires a complete change in the behavior of the network in the recruitment zone versus other parts of the cell. This in itself is not a fatal problem because such a change can be caused by a difference in the concentration of a cybernetic factor. The real problem is that there is simply no mechanism that obliges the network to march toward its demise in the recruitment zone in the first place. Since the recruitment zone by definition is a region of low contractility, the actual dynamical result is that the network flows out of the recruitment zone until it is completely contained in the region where contraction/gelation dominate. After this, all motion slowly grinds to a halt.

In our hands the only mechanism that is able to account for the steady cycling of network material between the endoplasm and ectoplasm requires the continuous synthesis and breakdown of the network. This is the same basic conclusion reached previously in our study of dissociated cytoplasm from amoebae (Dembo, 1986). In the minimal model, synthesis and breakdown are governed by the constitutive law for $\mathscr{J}$, Eq. 6a. This law, linear mass action, is certainly the simplest constitutive law one can imagine for such complex chemistry, yet it works remarkably well. We have tried to improve the minimal model by use of standard nonlinear reaction laws; some of these

(e.g., the logistic law) lead to oscillations in the total mass of network in the amoeba; others (e.g., autocatalytic destruction) are not outright refutable, but neither do they lead to substantial improvements.

The result of the synthesis-breakdown mechanism is to render meaningless the concept of a recruitment zone; it is even misleading to say that the network is "solated" or that the ectoplasm is somehow "converted" into endoplasm or vice versa. Events give the kinematic appearance of some validity of these concepts, but the real situation in the minimal model is that network in all portions of the cell is in a continuous dynamic equilibrium in which all its components cycle between polymerized and unpolymerized states. No particular spatial locations are preferred as far as either synthesis or breakdown are concerned. Simultaneously and independently, network filaments may flow into regions where they are at higher density and cross-linked or at lower density and less cross-linked. This is all.

If one has a model that yields a reasonable endoplasm-ectoplasm dichotomy and if there is also continuous flow of network material from the endoplasm to the ectoplasm, then the next problem is to explain how the endoplasm and ectoplasm become spatially distributed in the observed fashion. There are two fundamental anatomical "axes" that underlie the observed spatial distribution: the anterior-posterior axis and the cortico-medullary axis. An attempt to account for these organizational axes turns out to be quite important because it ultimately forces one to accept the existence of a cybernetic factor.

Without cybernetic factor one has to rely simply on the structure of the constitutive laws and the boundary conditions to stabilize the organizational axes. This sort of model is parsimonious from a mathematical point of view, and there is a very rich repertoire of meaningful variations. Furthermore, there is no rigorous logical argument for showing that such models must necessarily fail. Nevertheless, we have tried many models that do not involve cybernetic factor; they easily explain the anterior-posterior axis, but in every case the cortico-medullary axis is unstable. Clumps of ectoplasm clogging the endoplasm eventually occur, and it is thus impossible to obtain solutions corresponding to steady fountain flow. We believe that the basic reason for this is the fundamentally unnatural arrangement of the cortico-medullary axis.

If a contractile material is confined in a fixed domain of space, then it is intuitively clear that the "natural" tendency of the material is to form a clump somewhere in the middle. In contrast, what is seen in the amoeba (and also in other amoeboid cells) is a cortical shell of contractile material. This arrangement is basically unstable, and simply having "sticky" boundaries is not enough to keep things from falling apart. We should emphasize that we ourselves find the whole idea of cybernetic factors to be rather inelegant if not outright repulsive, but in the final analysis we simply cannot find a better (simpler) way of getting things to work.

Given the existence of some sort of cybernetic factor, one must address the question of how this factor operates. The factor could regulate the chemical reaction of network synthesis and breakdown ($\mathcal{A}$), the factor could control the viscosity of the network ($\mathcal{M}$), the factor could control the drag between the network and solution phases ($\mathcal{H}$), and the factor could work by controlling the network contractility ($\mathcal{C}$). At each of these control points the factor could act as a positive control (i.e., increasing viscosity, contractility, network synthesis, etc.) or as a negative control. Finally there are infinite possible nuances concerned with the exact functional form of the control relation (e.g., linear functions, step functions, etc.).

In the minimal model the only control point of the cybernetic factor is the network contractility, $\mathcal{C}$. This in itself seems to be quite important because we have been unsuccessful at obtaining good results with models in which $\mathcal{C}$ is not dependent on cybernetic factor. Nevertheless, the exact form of the control on $\mathcal{C}$ seems to be quite ambiguous. For example, we have obtained excellent results by replacing the positive-linear control law of the minimal model with a positive-logarithmic control law: $\mathcal{C} = \psi \, ln \, (q/\xi)$.

Another natural variation of the minimal model occurs if we replace the Dirichlet boundary conditions on q (Eq. 4e) by Neumann boundary conditions (Eq. 4d). Interestingly, this boundary condition works quite well despite considerable changes in the detailed distribution of the cybernetic factor close to the plasma membrane.

A more radical departure from the minimal model are models in which the cybernetic factor acts as a negative control on $\mathcal{C}$ rather than as a positive control. These models completely ignore the evidence that calcium is the cybernetic factor. They also require adjustments to the boundary conditions of q so that cybernetic factor is eliminated at the boundaries rather than supplied. In addition, it is necessary to adjust $\mathcal{S}$ so that q is supplied in the interior rather than destroyed. Nevertheless, in the final analysis negative control models can be made to work quite well.

The general lesson we draw is that if one wishes a stable cortico-medullary axis, one requires some sort of a cybernetic factor capable of causing $\mathcal{C}$ to get significantly larger in regions near the plasma membrane. Almost any control scheme that performs this function will be sufficient to account for all other aspects of fountain flow. In a way, it is remarkable that such a simple requirement is all that is needed to quash the inherent instability of the cortico-medullary axis. As a rather unfortunate corollary of this conclusion, the success of the minimal model

cannot be taken as support for the simple view that calcium is the cybernetic factor of *A. proteus* or for the particular version of calcium dynamics espoused by the model.

It is interesting to compare the simple contraction-coupled control mechanism in the minimal model with the hypothesis of solation-contraction coupling, (SCC), proposed by Hellewell and Taylor (1979). Both the minimal model and the SCC hypothesis view gelation as an effective break on contraction and solation as permissive of an increase in contraction. Both models also propose positive control of contraction by cybernetic factor. However, the SCC hypothesis also holds that cybernetic factor acts as a negative control of network viscosity. This hypothesis is supported by an observation that calcium and other putative cybernetic factors that stimulate contraction independently stimulate solation and vice versa. In the minimal model cybernetic factor stimulates contraction, which in turn stimulates gelation in a sequential fashion. As discussed above, this scheme plays the crucial role of limiting contraction and thereby allowing the differentiation of endoplasm and ectoplasm. If gelation is inhibited at sites of increased cybernetic factor, the result would be very counterproductive for the minimal model. Thus we are at a loss to explain the physiological role of negative coupling between cybernetic factor and network viscosity.

In contrast to the cortico-medullary distribution of network, there is nothing inherently unstable about the anterior-posterior distribution of network in fountain flow. Accordingly, the latter organizational axis can be explained simply by a difference in the "stickiness" of the inner surface of the plasma membrane for the network. Because the network cannot stick at the anterior, a weakness or opening occurs in the ectoplasmic layer. This then causes the ectoplasm to pull away and contract toward the tail, which in turn pushes the endoplasm forward. Thus in the minimal model the anterior-posterior axis results simply from the boundary conditions. This concept of how the anterior-posterior axis rises is similar to the "generalized cortical contraction" scheme proposed by Grebecki (1982).

Although boundary conditions can account for the anterior-posterior axis, mechanisms based on gradients of the cybernetic factor should be considered as well. An example of this sort of theory is the model of Pantin (1923). This model is based on the idea that protons enter the cell at the tips of pseudopods and that the resulting drop in local pH causes the liquefaction of the ectoplasm. Unfortunately Pantin does not seem to have worried about the basis of the cortico-medullary axis.

A more complete example of a model where a cybernetic factor is responsible for generating both the anterior-posterior and the cortico-medullary axes is obtained if one changes the anterior boundary condition of the minimal model from $q = 1$ to $q = 0$. Simultaneously, one may or may not change the anterior boundary condition on the network from no-stick to stick. Unfortunately, neither case explains the hyaline cap or the plasma gel sheet although an ectoplasmic tube and an acceptable pattern of fountain streaming are obtained. In general, it seems that the contractility of the network at the anterior must be vigorous to explain the hyaline cap and plasma gel sheet. Though models with weak anterior contractility can therefore be rejected as explanations of the monopodial form of *A. proteus*, the solutions they generate have some promise as models for pseudopodia that lack hyaline caps.

In view of the observation of a greater calcium concentration at the tail of monopodial amoebae (Taylor et al., 1980*a*), we have tried models in which there is a greater relative supply of cybernetic factor at $\partial \Omega_p$. This can be done in the context of either Dirichlet or Neumann boundary conditions. These models cannot be definitely refuted although they tend to produce too large an anterior-posterior gradient of network density.

The species name "*proteus*" derives from the Greek adjective for a deity capable of manifesting different forms. This name is very apt. For example, cylindrical specimens of *A. proteus* with two heads and specimens with two uroids have been well documented (Allen, 1961*b*). The reader will readily see that such monstrosities are easy to explain by simply changing the anterior or posterior boundary conditions in the minimal model. It is also easy to understand the phenomenon of "loop streaming" as a simple two-dimensional version of fountain streaming.

Another very well documented mode of cytoplasmic motion in a cylindrical amoeba has been termed "countercurrent streaming" by Allen (1973). The phenomenon has been filmed for an extended period in a specimen that was trapped in a cylindrical capillary and thus unable to alter geometry. Countercurrent streaming is characterized by breakup of the ectoplasmic tube into independent units or streamlets that flow backward at different rates and shear against each other. Although the bulk of the endoplasm streams forward, there are also streams of backward-moving material located in the middle of what is normally the endoplasmic channel, and having no apparent connection to the ectoplasm. In short, endoplasm and ectoplasm are still formed, but there has been a major breakdown of radial symmetry and of both cortico-medullary and anterior-posterior organization.

Allen has voiced the opinion that the occurrence of countercurrent streaming is rather difficult to explain theoretically. We must disagree with this conclusion since, as we have discussed at length, realistic models of the cytoplasm are inherently unstable. Chaotic modes (in

fact whole zoos full of chaotic modes) are a generic feature of these models (Dembo et al., 1984; Dembo, 1986). The essential conclusion is that, with appropriate parameter values, almost any model, including many that are much simpler than the minimal model, can explain relatively disorganized states like countercurrent streaming.

This work was supported by National Institutes of Health grants K04-AI00966 and R01-AI21002 and by the United States Department of Energy.

Received for publication 24 October 1988 and in final form 13 February 1989.

REFERENCES

Allen, R. D. 1960. The consistency of ameba cytoplasm and its bearing on the mechanism of ameboid movement. II. The effects of centrifugal acceleration observed in the centrifuge microscope. *J. Biophys. Biochem. Cytol.* 8:279–397.

Allen, R. D. 1961*a*. A new theory of amoeboid movement and protoplasmic streaming. *Exp. Cell Res. Suppl.* 8:17–31.

Allen, R. D. 1961*b*. Ameboid movement. *In* The Cell. Vol II. J. Brachet and A. E. Mirsky, editors. Academic Press, Inc., New York. 135–216.

Allen, R. D. 1973. Biophysical aspects of pseudopodium formation and retraction. *In* Biology of Amoeba. K. W. Jeon, editor. Academic Press, Inc., New York. 201–247.

Allen, R. D., and D. W. Francis. 1965. Cytoplasmic contraction and the distribution of water in the amoeba. *Soc. Exp. Biol. Symp.* 19:259–271.

Allen, R. D., and J. D. Roslansky. 1958. An anterior-posterior gradient of refractive index in the Ameba and its significance in amoeboid movement. *J. Biophys. Biochem. Cytol.* 4:517–525.

Allen, R. D., and J. D. Roslansky. 1959. The consistency of Ameba cytoplasm and its bearing on the mechanism of amoeboid movement. I. An analysis of endoplasmic velocity profiles of *Chaos chaos. J. Biophys. Biochem. Cytol.* 6:437–446.

Allen, R. D., and D. L. Taylor. 1975. The molecular basis of amoeboid movement. *In* Molecules and Cell Movement. S. Inoue and R. E. Stephens, editors. Raven Press, New York. 239–258.

Allen, R. D., J. W. Cooledge, and P. J. Hall. 1960. Streaming in cytoplasm dissociated from the giant amoeba, *Chaos chaos. Nature* (*Lond.*). 187:896–899.

Allen, R. D., R. R. Cowden, and P. J. Hall. 1962. Syneresis in ameboid movement: its localization by interference microscopy and its significance. *J. Cell Biol.* 12:185–189.

Astrand, P.-O., and K. Rodahl. 1986. Textbook of Work Physiology. McGraw-Hill Inc., New York.

Czarska, L., and A. Grebecki. 1966. Membrane folding and plasmamembrane ratio in the movement and shape transformation in *Amoeba proteus. Acta Protozool.* 4:201–239.

De Bruyn, P. P. H. 1947. Theories of amoeboid movement. *Q. Rev. Biol.* 22:1–24.

Dembo, M. 1986. The mechanics of motility in dissociated cytoplasm. *Biophys. J.* 50:1165–1183.

Dembo, M., and F. Harlow. 1986. Cell motion, contractile networks, and the physics of interpenetrating reactive flow. *Biophys. J.* 50:109–121.

Dembo, M., F. H. Harlow, and W. Alt. 1984. The biophysics of cell surface motility. *In* Cell Surface Dynamics: Concepts and Models. A. S. Perelson, C. DeLisi, and F. W. Wiegel, editors. Marcel Dekker, Inc., New York. 495–541.

Dembo, M., M. Maltrud, and F. Harlow. 1986. Numerical studies of unreactive contractile networks. *Biophys. J.* 50:123–137.

Dong, C., R. Skalak, K.-L. P. Sung, G. W. Schmid-Schonbein, and S. Chien. 1988. Passive deformation analysis of human leukocytes. *J. Biomech. Eng.* 110:27–36.

Evans, E. A., and B. Kukan, 1984. Passive material behavior of granulocytes based on large deformation and recovery after deformation tests. *Blood.* 64:1028–1035.

Grebecka, L. 1981. Motory effects of perforating peripheral cell layers of *Amoeba proteus. Protoplasma.* 106:343–349.

Grebecki, A. 1982. Supramolecular aspects of amoeboid movement. *Prog. Protozool. Proc. Int. Congr. Protozool.* 6:117–130.

Grebecki, A. 1984. Relative motion in *Amoeba proteus* in respect to the adhesion sites. I. Behavior of monotactic forms and the mechanism of fountain phenomenon. *Protoplasma.* 123:116–134.

Grebecki, A. 1987. Velocity distribution of the anterograde and retrograde transport of extracellular particles by *Amoeba proteus. Protoplasma.* 141:126–134.

Grebecki, A., and L. Grebecka. 1978. Morphodynamic types of *Amoeba proteus:* A terminological proposal. *Protistologica.* 14:349–358.

Griffin, J. L., and R. D. Allen. 1960. The movement of particles attached to the surface of amebae in relation to current theories of amoeboid movement. *Exp. Cell Res.* 20:619–622.

Happel, J., and H. Brenner. 1973. Low Reynolds Number Hydrodynamics. Noordhoff International, Leyden, Belgium.

Harlow, F. H., and J. E. Welch. 1965. Numerical calculation of time-dependent viscous incompressible flow. *Phys. Fluids.* 9:2182–2196.

Hellewell, S. B., and D. L. Taylor. 1979. The contractile basis of amoeboid movement. VI. The solation-contraction coupling hypothesis. *J. Cell Biol.* 83:633–648.

Hiramoto, Y. 1978. Mechanical properties of the dividing sea urchin egg. *In* Cell Motility: Molecules and Organization. S. Hatano, H. Ishikawa, and H. Sato, editors. University Park Press, Baltimore, MD. 653–663.

Kamiya, N. 1959. Protoplasmic streaming. *In* Protoplasmatologia, Handbuch der Protoplasmaforschung. Vol. 8. L. V. Heilbrunn and F. Weber, editors. Springer-Verlag, Vienna.

Kamiya, N., and K. Kuroda. 1958. Studies of the velocity distribution of the protoplasmic streaming in the myxomycete plasmodium. *Protoplasma.* 49:1–4.

Lovtrup, S., and A. Pigon. 1951. Diffusion and active transport of water in the amoeba *Chaos chaos L. Comptes Rendus des Travaux du Lab. Carlsberg, Ser. Chim.* 28:1–36.

Luby-Phelps, K., and D. L. Taylor. 1988. Subcellular compartmentalization by local differentiation of cytoplasmic structure. *Cell Motil. Cytoskeleton.* 10:28–37.

Mast, S. O. 1926. Structure, movement, locomotion, and stimulation in *Amoeba. J. Morph. Physiol.* 41:347–425.

Mast, S. O., and C. L. Prosser. 1932. Effect of temperature, salts, and hydrogen-ion concentration on rupture of the plasmagel sheet, rate of

locomotion, and gel/sol ratio in *Amoeba proteus*. *J. Cell. Comp. Physiol.* 1:333–354.

Nassberger, L., and M. Monti. 1984. Assessment of overall metabolism in *Amoeba proteus* measured by a microcalorimetric method. *Protoplasma.* 123:135–139.

Odell, G. M. 1977. Amoeboid motions. *Lect. Appl. Math.* 16:191–220.

Opas, M. 1980. Cytoplasmic streaming: is the steam in amoeba really homogeneous? *Bull. Acad. Pol. Sci. Ser. Sci. Biol.* 28:515–519.

Pantin, C. F. A. 1923. On the physiology of amoeboid movement. *J. Mar. Biol. Assoc.* 13:24–69.

Pollard, T. D., and S. Ito. 1970. Cytoplasmic filaments of *Amoeba proteus*. I. The role of filaments in consistency changes and movement. *J. Cell Biol.* 46:267–289.

Pollard, T. D., and E. D. Korn. 1971. Filaments of *Amoeba proteus*. II. Binding of heavy meromyosin by thin filaments in motile cytoplasmic extracts. *J. Cell Biol.* 48:216–219.

Pracht, W. E. 1971. A numerical method for calculating transient creep flows. *J. Comp. Phys.* 7:46–60.

Rinaldi, R. A., W. Korohoda, and K. E. Wholfarth-Botterman. 1975. Some effects of externally applied pressure upon cytoplasmic movement in the amoeba *Chaos chaos*. *Acta Protozool.* 14:363–369.

Sato, M., T. Z. Wong, and R. D. Allen. 1983. Rheological properties of living cytoplasm: endoplasm of *Physarum* plasmodium. *J. Cell Biol.* 97:1089–1097.

Stoer, J. 1983. Solution of large linear systems of equations by conjugate gradient type methods. *In* Mathematical Programming: The State of the Art. A. Bachem, M. Grotschel, and B. Korte, editors. Springer-Verlag, New York. 540–565.

Taylor, D. L. 1976. Motile model systems of amoeboid movement. *In* Cell Motility. Cold Spring Harbor Conference on Cell Proliferation. Vol. 3. R. Goldman, T. Pollard, and J. Rosenbaum, editors. Cold Spring Harbor Laboratory, Cold Spring Harbor, NY. 797–822.

Taylor, D. L., and J. S. Condeelis. 1979. Cytoplasmic structure and contractility in amoeboid cells. *Int. Rev. Cytol.* 56:57–114.

Taylor, D. L., J. S. Condeelis, P. L. Moore, and R. D. Allen. 1973. The contractile basis of amoeboid movement. I. The chemical control of motility in isolated cytoplasm. *J. Cell Biol.* 59:378–394.

Taylor, D. L., J. R. Blinks, and G. Reynolds. 1980*a*. Contractile basis of amoeboid movement. VIII. Aequorin luminescence during ameboid movement, endocytosis, and capping. *J. Cell Biol.* 86:599–602.

Taylor, D. L., Y.-L. Wang, and J. M. Heiple. 1980*b*. Contractile basis of ameboid movement. VII. The distribution of fluorescently labeled actin in living amebas. *J. Cell Biol.* 86:590–598.

Wang, Y.-L., F. Lanni, P. L. McNeil, B. R. Ware, and D. L. Taylor. 1982. Mobility of cytoplasmic and membrane-associated actin in living cells. *Proc. Natl. Acad. Sci. USA.* 79:4660–4664.

Yagi, K. 1961. The mechanical and colloidal properties of amoeba protoplasm and their relations to the mechanism of amoeboid movement. *Comp. Biochem. Physiol.* 3:73–91.

Young, D. M. 1971. Iterative Solution of Large Linear Systems. Academic Press, Inc., New York.